Three-body calculations of β decay applied to ^{11}Li

E. Garrido [,1] A. S. Jensen,[2] H. O. U. Fynbo [,2] and K. Riisager [2]

[1]*Instituto de Estructura de la Materia, CSIC, Serrano 123, E-28006 Madrid, Spain*
[2]*Department of Physics and Astronomy, Aarhus University, DK-8000 Aarhus C, Denmark*

A novel practical few-body method is formulated to include isospin symmetry for nuclear halo structures. The method is designed to describe β decay, where the basic concept of isospin symmetry facilitates a proper understanding. Both isobaric analog and antianalog states are treated. We derive general and explicit formulas for three-body systems using hyperspherical coordinates. The example of the β decaying ^{11}Li (^{9}Li $+ n + n$) is chosen as a challenging application for numerical calculations of practical interest. The detailed results are compared to existing experimental data, and good agreement is found at high excitation energies, where the isobaric analog and antianalog states are situated in the daughter nucleus. An interpretation of the decay pattern at lower excitation energies is suggested. Decays of the ^{9}Li core and the two halo neutrons are individually treated and combined with the daughter system with almost unique isospin, which we predict to be broken by about 0.4% probability. Properties of decay products are predicted as possible future tests of this model.

I. INTRODUCTION

Nuclear halo states are characterized by a significant decoupling of the halo particle(s) from the remainder of the nucleus [1,2]. Many accounts of halo nuclei focus on the spatial decoupling of the halo and the core, but the decoupling of dynamic degrees of freedom is of similar importance. This has implications for many aspects of their structure and for the dynamics when undergoing nuclear reactions. The aim of the current paper is to explore how β decay of halo nuclei is affected through the use of a few-body model that enables treatment also of the continuum behavior.

Most established halo states are ground states of light nuclei in the vicinity of the neutron or proton drip lines. Here β decay energies are large, and allowed transitions dominate the decay pattern; see [3,4] for general overviews. β decays are a valuable probe of nuclear structure with operators that for allowed transitions do not involve the spatial coordinates. The decays of halo nuclei are reviewed in a recent paper [5], and two specific features are important for the current work. The first is that the large spatial extension of the halo wave functions can give rise to decays that are most efficiently described as proceeding directly to continuum states, as done naturally in few-body models. The second is that the decoupling between halo and core may lead to distinct patterns in the decay as discussed in the next section. It should be recalled that the physics structure is often seen best in transitions of large β strength that only rarely correspond to those with high branching ratio.

The nucleus ^{11}Li is not only one of the best studied halo nuclei, but also has a very diverse breakup pattern during the β decay process [5], and it is therefore natural to take a close look at this decay. Furthermore, it has been difficult to pin down the many decay branches of the nucleus, not only experimentally, but also from the theoretical point of view. This is connected to the fact that most of the β strength in the ^{11}Li decay leads to breakup into continuum states. For example, with the shell model [6,7] or the antisymmetrized molecular dynamics [8], the calculations are often restricted to the β strength distribution in ^{11}Be, and they do not attempt to describe the subsequent particle emission or the coupling to the continuum. The only exception is calculations [9–11] of the β-delayed deuteron branch that assume decays direct to the continuum.

In this work, we shall investigate the β decay of the ^{11}Li nucleus in its ground state. The calculations will be based on a three-body framework (core plus two halo nucleons), by means of the hyperspherical adiabatic expansion method [12]. Earlier the method was used to describe not only ^{11}Li, but also its mirror nucleus ^{11}O, the two extremes of a $T = 5/2$ isospin multiplet [13]. We now extended this two- and three-body general formulation to treat the isospin symmetry fully and consistently for other less extreme members of the multiplet. The extension to multiplet members in between, such as the isobaric analog state (IAS) or the antianalog state (AAS) in ^{11}Be, will be considered in detail. We shall provide the necessary technical developments to be implemented into the standard three-body method. The extended method also allows one to determine which asymptotic channels the decays proceed through.

After this introduction, we start in Sec. II by outlining isospin structures and concepts in the β decay process that are the basis of the subsequent sections. The general numerical three-body method used in the calculations and, in particular, the new implementation of the isospin degrees of freedom will be described in Sec. III. In Sec. IV, we focus on the particular

case of ^{11}Li, describing the isospin structure of the wave functions, matrix elements, and energies. In Secs. V and VI we continue with the corresponding numerical calculations of, respectively, three-body wave functions and β decay strength. A comparison to the experimentally established decay scheme follows in Sec. VII. Finally, we conclude in Sec. VIII with a brief outlook. Some technical details and supplementary information are given in appendices.

II. CONCEPTUAL BACKGROUND

We use the convention where the neutron has third isospin component $-\frac{1}{2}$. The operators for allowed Fermi and Gamow-Teller $\beta^{\mp}$ decay then have the form $\hat{\mathcal{O}}_F^{\mp} = \sum_i t_i^{\pm} = T^{\pm}$ and $\hat{\mathcal{O}}_{GT}^{\mp} = \sum_i \boldsymbol{\sigma}_i t_i^{\pm}$; here $\boldsymbol{t}_i$ and $\boldsymbol{\sigma}_i \hbar/2$ are, respectively, the isospin and spin operators acting on nucleon i, and $\boldsymbol{T}$ is the total isospin operator of the nucleus. The ladder operator t_i^+ is defined as $t_i^+ = t_{x_i} + i t_{y_i}$, where t_{x_i} and t_{y_i} are the Cartesian x and y components of the vector operator $\boldsymbol{t}_i$.

A. Core and halo decays

Let us consider first the case where a halo state has one or more neutrons in the halo component (the modifications to proton halos are then trivial) and that the mass numbers of the core and halo components are A_c and A_h with total mass number $A = A_c + A_h$. The total isospin is split into core and halo parts, $\boldsymbol{T} = \boldsymbol{t_c} + \boldsymbol{t_h}$, and we can assume that the quantum numbers fulfill $t_h = A_h/2$, $T = t_c + t_h$, whose respective third components are given by $T_z = -T$, $t_c^z = -t_c$, $t_h^z = -t_h$.

Our basic approximation is taken from [14,15]. It is applicable for pronounced halo states where the wave function can be factorized into a core and a halo part. An allowed β-decay operator $\hat{\mathcal{O}}_\beta^A$, either Fermi or Gamow-Teller, is a sum over operators for each nucleon. Therefore, one formally can divide the sum into two components, corresponding to core decay and halo decay:

$$\hat{\mathcal{O}}_\beta^A |c+h\rangle = \hat{\mathcal{O}}_\beta^A(|c\rangle|h\rangle) = |c\rangle\left(\hat{\mathcal{O}}_\beta^{A_h}|h\rangle\right) + \left(\hat{\mathcal{O}}_\beta^{A_c}|c\rangle\right)|h\rangle, \quad (1)$$

where $|c\rangle$ and $|h\rangle$ represent the (decoupled) core and halo parts of the wave function.

As illustrated shortly, the two final components will in general not have an individual well-defined isospin. Furthermore, the core-decay component often contains several terms corresponding to different levels in its daughter nucleus. Therefore, the right-hand side in general does not give eigenstates in the final system, but may suggest a skeleton to be used in interpreting patterns in the β decay. Some experimental support for our approximation is found in the decays of the halo nuclei ^{6}He ($\alpha + 2n$) and ^{14}Be (^{10}Be $+4n$) [5,14,15]: in the former case $t_c = 0$ and the decay is a pure halo decay, in the latter case the main decay branch (to a low-lying 1^+ level in ^{14}B) is very similar to the decay of the ^{12}Be core so this branch looks like a "core decay."

Our procedure will then be to calculate the initial wave function in a few-body model that includes all halo degrees of freedom, and act on it with the β decay operators according to Eq. (1). The resulting wave function then must be projected on the final states. Our computational challenge is not to find

an accurate halo wave function, but to obtain a realistic description of the final states. The main simplifying assumption is to assume few-body structures in the final states also, and calculate these in a similar manner, but of course with adjusted interactions. This cannot be expected to reproduce all details of the final states, but may provide the main features of how the β strength is distributed in energy and thus could be a good approximation for the components with large β strength.

B. Isospin, IAS, and AAS

Isospin is a good quantum number for most nuclear states and is particularly relevant for β decay, since the operator for allowed Fermi decay is simply the isospin raising/lowering operator. We refer to Appendix A for a more extensive discussion and give here the relevant wave functions for the general (neutron-rich) halo system considered above. The notation reflects that we shall mainly be interested in two-neutron halo nuclei where the isospins of the halo nucleons, t_2 and t_3, couple to the halo isospin, t_h, which in turn couples to the core isospin, t_c, to give the total isospin, T, with projection T_z.

The isospin wave functions are then for the halo state, the isobaric analog state (IAS), and the corresponding antianalog state (AAS), given by

$$|\text{halo}\rangle = |(t_2, t_3)t_h, t_c; T = t_h + t_c, T_z = -t_h - t_c\rangle$$
$$= \left|t_c, t_c^z = -t_c\right\rangle\left|t_h, t_h^z = -t_h\right\rangle, \quad (2)$$

$$|\text{IAS}\rangle = |(t_2, t_3)t_h, t_c; T = t_h + t_c, T_z = -t_h - t_c + 1\rangle$$
$$= \sqrt{\frac{t_h}{t_c + t_h}}\left|t_c, t_c^z = -t_c\right\rangle\left|t_h, t_h^z = -t_h + 1\right\rangle$$
$$+ \sqrt{\frac{t_c}{t_c + t_h}}\left|t_c, t_c^z = -t_c + 1\right\rangle\left|t_h, t_h^z = -t_h\right\rangle, \quad (3)$$

and

$$|\text{AAS}\rangle = |(t_2, t_3)t_h, t_c; T = t_h + t_c - 1, T_z = -t_h - t_c + 1\rangle$$
$$= \sqrt{\frac{t_c}{t_c + t_h}}\left|t_c, t_c^z = -t_c\right\rangle\left|t_h, t_h^z = -t_h + 1\right\rangle$$
$$- \sqrt{\frac{t_h}{t_c + t_h}}\left|t_c, t_c^z = -t_c + 1\right\rangle\left|t_h, t_h^z = -t_h\right\rangle, \quad (4)$$

where t_c^z and t_h^z are the projections of t_c and t_h, respectively. If $t_c = 0$ only the IAS exists and it is given by the first term in Eq. (3). Note that whereas the IAS normally remains quite pure, the AAS will often be close to states in the daughter nucleus with the same (lower) isospin, spin, and parity and may mix with those states.

III. NUMERICAL THREE-BODY METHOD

In this work we assume that the nuclei involved in our investigation can be described as a core surrounded by two halo nucleons. Therefore, together with the three-body method itself, all the required internal two-body interactions need to be specified. On top of that, the decays of the core and nucleon halo have to be both considered.

A. Formulation

The total three-body wave function describing the system will be obtained by means of the hyperspherical adiabatic expansion method detailed in [12]. According to this method the three-body wave functions are written as

$$\Psi(\boldsymbol{x}, \boldsymbol{y}) = \frac{1}{\rho^{5/2}} \sum_n f_n(\rho) \Phi_n(\rho, \Omega), \tag{5}$$

where $\boldsymbol{x}$ and $\boldsymbol{y}$ are the usual Jacobi coordinates, from which one can define the hyperradius ρ and the five hyperangles (collected into Ω) [12]. The angular functions $\Phi_n(\rho, \Omega)$ are the eigenfunctions of the angular part of the Schrödinger, or Faddeev, equations, with eigenvalues $\lambda_n(\rho)$. The radial functions, $f_n(\rho)$, are obtained as the solution of a coupled set of differential equations in which the angular eigenvalues, $\lambda_n(\rho)$, enter as effective potentials:

$$V_{\text{eff}}(\rho) = \frac{\hbar^2}{2m} \frac{\lambda_n(\rho) + \frac{15}{4}}{\rho^2}, \tag{6}$$

where m is the arbitrary normalization mass used to construct the Jacobi coordinates [12].

In the calculations, the angular eigenfunctions Φ_n are expanded in terms of the basis set $\{|\mathcal{Y}_q\rangle\}$, where $\mathcal{Y}_q$ represents the coupling between the usual hyperspherical harmonics and the spin terms, and where q collects all the necessary, orbital and spin, quantum numbers. The number of components, as well as the number of terms in the expansion in Eq. (5), should of course be large enough to get a converged three-body wave function.

The calculations, as described in Ref. [12], have now to be extended to make explicit the isospin quantum numbers associated to the system under investigation. As mentioned above, the isospin state of the halo system, the IAS, and the AAS, are given by the isospin wave functions specified in Eqs. (2), (3), and (4), respectively. The isospin quantum numbers characterize each of the states to be computed. With this in mind, the simplest procedure to incorporate the isospin state into the calculation is to proceed as described in [12], but where the basis set used for the expansion of the angular eigenfunctions, Φ_n, is not just given by the $\{|\mathcal{Y}_q\rangle\}$ terms formed after the coupling of the hyperspherical harmonics and the spin functions, but by the set $\{|\mathcal{Y}_q\rangle|T T_z\rangle\}$, where $|T T_z\rangle \equiv |(t_2 t_3) t_h, t_c; T T_z\rangle$ is the isospin function of the system to be computed.

In other words, following the procedure sketched above, the full three-body wave function, Ψ, is in practice written as

$$\Psi = \Psi_{3b} |T T_z\rangle, \tag{7}$$

where Ψ_{3b} describes the relative motion between the three constituents of the system.

B. Core energy

An important point to take into account is that the total Hamiltonian is actually the sum of the one describing the relative motion of the three constituents of the system, plus the core Hamiltonian, $\mathcal{H}_{\text{core}}$, which describes the core degrees

of freedom. The Hamiltonian $\mathcal{H}_{\text{core}}$ is such that

$$\mathcal{H}_{\text{core}} |t_c, t_c^z\rangle = \xi_{\text{core}} |t_c, t_c^z\rangle, \tag{8}$$

where ξ_{core} is the energy of the core.

Obviously, in order to obtain the three-body wave function, the diagonalization of the full hamiltonian will require inclusion of the all the matrix elements of $\mathcal{H}_{\text{core}}$ between all the elements of the basis set used for the expansion, $\{|\mathcal{Y}_q\rangle|T T_z\rangle\}$. Making use of Eqs. (2), (3), and (4), we can easily see that these matrix elements for the halo states, the IAS, and the AAS, are given by

$$\langle \mathcal{Y}_q; \text{halo} | \mathcal{H}_{\text{core}} | \mathcal{Y}_{q'}; \text{halo} \rangle = \xi_{-t_c} \delta_{qq'}, \tag{9}$$

$$\langle \mathcal{Y}_q; \text{IAS} | \mathcal{H}_{\text{core}} | \mathcal{Y}_{q'}; \text{IAS} \rangle$$
$$= \left(\frac{t_h}{t_c + t_h} \xi_{-t_c} + \frac{t_c}{t_c + t_h} \xi_{-t_c+1} \right) \delta_{qq'}, \tag{10}$$

and

$$\langle \mathcal{Y}_q; \text{AAS} | \mathcal{H}_{\text{core}} | \mathcal{Y}_{q'}; \text{AAS} \rangle$$
$$= \left(\frac{t_c}{t_c + t_h} \xi_{-t_c} + \frac{t_h}{t_c + t_h} \xi_{-t_c+1} \right) \delta_{qq'}, \tag{11}$$

where ξ_{-t_c} and ξ_{-t_c+1} are, respectively, the energies of the core represented by the $|t_c, t_c^z = -t_c\rangle$ and $|t_c, t_c^z = -t_c + 1\rangle$ isospin states.

Usually, individual three-body energies are referred to the three-body threshold, which amounts to taking $\xi_{\text{core}} = 0$. However, when comparing the energy between different three-body systems, a unique zero energy point has to be chosen, which implies that, when different cores are involved, only the energy of one of them can be taken equal to zero, whereas the energy of the other ones has to be referred to the first one.

As we can see, the effect of the core Hamiltonian is a shift of the effective potentials, different for the halo state, the IAS, and the AAS, and which is dictated by the core energies. We have assumed that $\mathcal{H}_{\text{core}}$ does not mix the $|t_c, t_c^z = -t_c\rangle$ and $|t_c, t_c^z = -t_c + 1\rangle$ core states.

C. Potential matrix elements

At this point it should be noticed that the isospin wave functions in Eqs. (2), (3), and (4) explicitly show the three-body structures involved in each case, with a core described by the isospin state $|t_c, t_c^z\rangle$, and a halo state described by $|t_h, t_h^z\rangle$. In particular, the halo state contains a single configuration with the core and the halo in the $|t_c, t_c^z = -t_c\rangle$ and the $|t_h, t_h^z = -t_h\rangle$ isospin states, respectively. In contrast, the IAS and AAS mix two configurations, one with the core and the halo in the $|t_c, t_c^z = -t_c\rangle$ and $|t_h, t_h^z = -t_h + 1\rangle$ isospin states, and the other one with the core and the halo in the $|t_c, t_c^z = -t_c + 1\rangle$ and $|t_h, t_h^z = -t_h\rangle$ isospin states.

In any case, in order to perform the calculations, this decomposition of the isospin states is not the most convenient one. This is because the core-nucleon interactions will in general depend on the total core-nucleon isospin, t_{cN}, resulting from the coupling between the core and nucleon isospins. For this reason, it is preferable to rotate the isospin wave function $|(t_2, t_3) t_h, t_c; T, T_z\rangle$, which is written in what

we usually call the first Jacobi set (or T set), into the second or third Jacobi sets (Y sets), where the core and the nucleon isospins are first coupled into t_{cN}, and then coupled to the isospin of the second halo nucleon in order to produce the total isospin T of the system. In this way, the dependence of the isospin wave functions on t_{cN} appears explicitly. In particular, when rotating into the second Jacobi set we get

$$|(t_2, t_3)t_h, t_c; T, T_z\rangle = (-1)^{t_c + t_2 + t_3} \sum_{t_{cN}} (-1)^{t_{cN} + t_2} \sqrt{2t_{cN} + 1} \sqrt{2t_h + 1} \begin{Bmatrix} t_3 & t_2 & t_h \\ T & t_c & t_{cN} \end{Bmatrix} |(t_3, t_c)t_{cN}, t_2; T, T_z\rangle, \quad (12)$$

which makes evident that the isospin states given in Eqs. (2), (3), and (4), can, in general, mix different values of the core-nucleon isospin, t_{cN}. The curly brackets denote the six-j symbol.

When solving the three-body problem, it is always necessary at some point to compute the matrix elements of the two-body potentials between the different terms of the basis set used in the expansion of the wave function, $\{|\mathcal{Y}_q\rangle|TT_z\rangle\}$. Thanks to the expression in Eq. (12), and assuming that the core-nucleon potential, V_{cN}, does not mix different t_{cN} values, we easily get for the potential matrix elements

$$\langle \mathcal{Y}_q; T, T_z | V_{cN} | \mathcal{Y}_{q'}; T, T_z \rangle = \sum_{t_{cN}} (2t_{cN} + 1)(2t_h + 1) \begin{Bmatrix} t_3 & t_2 & t_h \\ T & t_c & t_{cN} \end{Bmatrix}^2 \langle \mathcal{Y}_q; (t_3, t_c)t_{cN}, t_2; T, T_z | V_{cN}^{(t_{cN})} | \mathcal{Y}_{q'}; (t_3, t_c)t_{cN}, t_2; T, T_z \rangle, \quad (13)$$

where we can see that the calculation of the different core-nucleon potential matrix elements requires knowledge of the potentials for the different possible values of t_{cN}, i.e., knowledge of all the possible $V_{cN}^{(t_{cN})}$ potentials.

Furthermore, in order to fully determine the potential matrix elements, it is also necessary to decouple t_3 and t_c, such that the values of the third isospin components, t_3^z and t_c^z, are made explicit. This is required in order to know what precise core state and nucleon state are actually interacting. After doing this we get

$$\langle \mathcal{Y}_q; (t_3, t_c)t_{cN}, t_2; T, T_z | V_{cN}^{(t_{cN})} | \mathcal{Y}_{q'}; (t_3, t_c)t_{cN}, t_2; T, T_z \rangle$$
$$= \sum_{t_{cN}^z t_2^z} \langle t_{cN} t_2; t_{cN}^z t_2^z | T T_z \rangle^2 \sum_{t_c^z t_3^z} \langle t_3 t_c; t_3^z t_c^z | t_{cN}, t_{cN}^z \rangle^2 \langle \mathcal{Y}_q; t_c t_c^z; t_3 t_3^z | V_{cN}^{(t_{cN})} | \mathcal{Y}_{q'}; t_c t_c^z; t_3 t_3^z \rangle, \quad (14)$$

which, after insertion into Eq. (13), gives the details of the required potential matrix elements. The matrix element $\langle \mathcal{Y}_q; t_c t_c^z; t_3 t_3^z | V_{cN}^{(t_{cN})} | \mathcal{Y}_{q'}; t_c t_c^z; t_3 t_3^z \rangle$ refers to the matrix element between the basis elements $\mathcal{Y}_q$ and $\mathcal{Y}_{q'}$, when the core is in the $|t_c, t_c^z\rangle$ isospin state and the nucleon in the $|t_3, t_3^z\rangle$ state, coupled to the two-body isospin t_{cN}, and interacting via the potential $V_{cN}^{(t_{cN})}$. We have assumed here that the potential does not mix different isospin states.

Therefore, in order to describe a particular system, all the core-nucleon potentials required to compute all the possible $\langle \mathcal{Y}_q; t_c t_c^z; t_3 t_3^z | V_{cN}^{(t_{cN})} | \mathcal{Y}_{q'}; t_c t_c^z; t_3 t_3^z \rangle$ matrix elements need to be specified. Once this is done, we can then compute the three-body wave function, Ψ_{3b}, entering in Eq. (7) as described in Eq. (5), which contains the isospin dependence of the potentials through the matrix elements in Eqs. (13) and (14), as well as the dependence on the excitation energy of the core through the matrix elements in Eqs. (9) to (11).

D. β decay strength

Let us now consider the β decay of some initial state $\Psi^{(\mathrm{in})} = \Psi_{3b}^{(\mathrm{in})}|T', T_z'\rangle$ by the action of the β decay operator $\hat{\mathcal{O}}_\beta^A$, as given in Eq. (1), and project on some final state $\Psi^{(\mathrm{fin})} = \Psi_{3b}^{(\mathrm{fin})}|T, T_z\rangle$, where $|T', T_z'\rangle$ and $|T, T_z\rangle$ describe the respective initial and final isospin states.

For Fermi and Gamow-Teller decays the corresponding transition strengths are given by

$$B = \frac{1}{2J_i + 1} |\langle \Psi_{3b}^{(\mathrm{fin})} || \langle T, T_z | \hat{\mathcal{O}}_\beta^A | T', T_z' \rangle || \Psi_{3b}^{(\mathrm{in})} \rangle|^2, \quad (15)$$

where $\hat{\mathcal{O}}_\beta^A$ is either the Fermi, $\mathcal{O}_F^\mp = \sum_j t_j^\pm$, or Gamow-Teller, $\mathcal{O}_{GT}^\mp = \sum_j \boldsymbol{\sigma}_j t_j^\pm$, decay operator, and where J_i is the angular momentum quantum number of the initial state and j runs over all the A nucleons of the initial system.

As shown in Eq. (1), the Fermi and Gamow-Teller operators can be split in two pieces, the first one involving the decay of the valence nucleons and the second one involving the decay of the core nucleons. In this way, the reduced matrix elements contained in Eq. (15) can be written as

$$\langle \Psi_{3b}^{(\mathrm{fin})} || \langle T, T_z | \hat{\mathcal{O}}_\beta^A | T', T_z' \rangle || \Psi_{3b}^{(\mathrm{in})} \rangle$$
$$= \langle \Psi_{3b}^{(\mathrm{fin})} || \langle T, T_z | \hat{\mathcal{O}}_\beta^{A_h} | T', T_z' \rangle || \Psi_{3b}^{(\mathrm{in})} \rangle$$
$$+ \langle \Psi_{3b}^{(\mathrm{fin})} || \langle T, T_z | \hat{\mathcal{O}}_\beta^{A_c} | T', T_z' \rangle || \Psi_{3b}^{(\mathrm{in})} \rangle, \quad (16)$$

where

$$\hat{\mathcal{O}}_\beta^{A_h} = \sum_{j=v_1, v_2} t_j^\pm \quad \text{or} \quad \hat{\mathcal{O}}_\beta^{A_h} = \sum_{j=v_1, v_2} \boldsymbol{\sigma}_j t_j^\pm \quad (17)$$

describes the Fermi or Gamow-Teller decay of the halo nucleons, denoted by v_1 and v_2, and

$$\hat{\mathcal{O}}_\beta^{A_c} = \sum_{j \in \mathrm{core}} t_j^\pm \quad \text{or} \quad \hat{\mathcal{O}}_\beta^{A_c} = \sum_{j \in \mathrm{core}} \boldsymbol{\sigma}_j t_j^\pm \quad (18)$$

describes the Fermi or Gamow-Teller decay of the A_c nucleons in the core.

From Eqs. (2), (3), and (4), it is simple to see that the core isospin matrix element in the equation above

becomes

$$\langle \text{halo}; T, T_z | \hat{\mathcal{O}}_\beta^{A_c} | \text{halo}; T', T'_z \rangle$$
$$= \langle t_c, t_c^z = -t_c | \hat{\mathcal{O}}_\beta^{A_c} | t'_c, t_c^{'z} = -t'_c \rangle, \qquad (19)$$

$$\langle \text{IAS}; T, T_z | \hat{\mathcal{O}}_\beta^{A_c} | \text{halo}; T', T'_z \rangle$$
$$= \sqrt{\frac{t_c}{t_c + t_h}} \langle t_c, t_c^z = -t_c + 1 | \hat{\mathcal{O}}_\beta^{A_c} | t'_c, t_c^{'z} = -t'_c \rangle, \quad (20)$$

or

$$\langle \text{AAS}; T, T_z | \hat{\mathcal{O}}_\beta^{A_c} | \text{halo}; T', T'_z \rangle$$
$$= -\sqrt{\frac{t_h}{t_c + t_h}} \langle t_c, t_c^z = -t_c + 1 | \hat{\mathcal{O}}_\beta^{A_c} | t'_c, t_c^{'z} = -t'_c \rangle, \quad (21)$$

which permit to write the reduced β decay matrix element Eq. (16) as

$$\langle \Psi_{3b}^{(\text{fin})} || \langle T, T_z | \hat{\mathcal{O}}_\beta^A | T', T'_z \rangle || \Psi_{3b}^{(\text{in})} \rangle$$
$$= \langle \Psi_{3b}^{(\text{fin})} || \langle T, T_z | \hat{\mathcal{O}}_\beta^{A_h} | T', T'_z \rangle || \Psi_{3b}^{(\text{in})} \rangle$$
$$+ f_{\text{fin}} \langle \Psi_{3b}^{(\text{fin})} || \Psi_{3b}^{(\text{in})} \rangle \langle t_c, t_c^z | \hat{\mathcal{O}}_\beta^{A_c} | t'_c, t_c^{'z} \rangle, \qquad (22)$$

where $f_{\text{fin}} = 1, \sqrt{t_c/(t_c + t_h)}$, or $-\sqrt{t_h/(t_c + t_h)}$, depending on the character (halo state, IAS, or AAS) of the final state, and where $\langle \Psi_{3b}^{(\text{fin})} || \Psi_{3b}^{(\text{in})} \rangle$ is the overlap of the initial and final three-body wave functions, excluding the isospin part. The final matrix element describes the β decay of the core, whose initial and final isospin states are given by $|t'_c, t_c^{'z}\rangle$ and $|t_c, t_c^z\rangle$, respectively.

For Fermi decay, the transition operator depends on the isospin only. It is then possible to factorize the matrix element $\langle \Psi_{3b}^{(\text{fin})} || \langle T, T_z | \hat{\mathcal{O}}_\beta^{A_h} | T', T'_z \rangle || \Psi_{3b}^{(\text{in})} \rangle$ into one term involving only the coordinate and spin parts of the initial and final three-body wave functions [Ψ_{3b} in Eq. (7)], and another matrix element involving only the isospin part. In other words, for Fermi decay we can write

$$\langle \Psi_{3b}^{(\text{fin})} || \langle T, T_z | \sum_{j=1}^A t_j^+ | T, T'_z \rangle || \Psi_{3b}^{(\text{in})} \rangle$$
$$= \langle \Psi_{3b}^{(\text{fin})} || \Psi_{3b}^{(\text{in})} \rangle \Bigg(\langle T, T_z | \sum_{j=v_1, v_2} t_j^+ | T', T'_z \rangle$$
$$+ f_{\text{fin}} \langle t_c, t_c^z | \sum_{j \in \text{core}} t_j^+ | t'_c, t_c^{'z} \rangle \Bigg), \qquad (23)$$

which means that the Fermi decay matrix element is given just by the overlap of the initial and final three-body wave functions (excluding the isospin part) times an isospin dependent global factor.

E. Contribution from the continuum background

The matrix elements derived in the previous section correspond to the β decay transition from some halo initial state into some halo or IAS or AAS final state, each characterized by specific isospin quantum numbers. However, when computing the strength for a particular transition, it is necessary to include the contribution from transitions into the continuum

states having the same quantum numbers as the final state, either halo state, IAS, or AAS.

In this work the continuum states will be computed as discrete states after imposing a box boundary condition. In other words, for a given set of quantum numbers, the radial wave functions in Eq. (5) are obtained by solving the radial part of the three-body equations in a box with a sufficiently large maximum value for the hyperradius. To be specific, we shall use the finite-difference method described for instance in Chap. 19 of Ref. [16]. This method permits to reduce the system of coupled differential equations into an eigenvalue problem, such that the eigenfunctions are the radial solutions evaluated at specific chosen values of the radial coordinate, and the eigenvalues are the "discrete" continuum energies.

In this way, together with the precise three-body wave function for the final state (halo state, IAS, or AAS), we get, for each of them, a family of "discrete" continuum states with the same quantum numbers. Therefore, the total transition strength to the states with a definite set of quantum numbers will be given by the sum of all the strengths given in Eq. (15) for Fermi or Gamow-Teller strengths, respectively. Of course, the sum runs over all the computed discrete states.

At this point it is also interesting to consider the differential transition strength, which permits to obtain the distribution of the strength as a function of the final three-body energy. When dealing with discrete states, and following Eq. (15), we can easily write the differential transition strength for Fermi and Gamow-Teller transitions as

$$\frac{dB}{dE} = \frac{1}{2J_i + 1} \sum_k \delta(E - E_k)$$
$$\times \left| \langle \Psi_{3b}^{(\text{fin})}(E_k) || \langle T, T_z | \hat{\mathcal{O}}_\beta^A | T', T'_z \rangle || \Psi_{3b}^{(\text{in})} \rangle \right|^2, \quad (24)$$

where k runs over all the discrete final states, with energy E_k and wave function $\Psi_{3b}^{(\text{fin})}(E_k)$. The integral over the three-body energy, E, trivially provides the total strength, and the reduced matrix elements for the Fermi and Gamow-Teller decays are given by Eq. (22), which for Fermi decay can be simplified into Eq. (23).

In our calculations the δ function will be replaced by the normalized Gaussian

$$\delta(E - E_k) \approx \frac{1}{\sqrt{2\pi}\sigma} e^{-\frac{(E - E_k)^2}{2\sigma^2}}, \qquad (25)$$

where the Gaussian width, σ, is made as small as possible while producing a smooth strength function [otherwise Eq. (24) would become a sequence of delta functions located at the energies of the different discrete states]. Typical σ values range within the interval $\sigma = 0.1$ MeV and $\sigma = 0.3$ MeV and therefore larger than the distance between the discrete continuum states, which, in our calculations, will be in the range of 0.05 to 0.1 MeV.

IV. APPLICATION TO ^{11}Li β DECAY

We shall here employ the extended three-body formalism described in the previous section to investigate β decay of the ^{11}Li ground state. After specifying the isospin formalism in

the context, we proceed to calculate energies, potentials and wave functions.

A. Specific information

In the following we denote the ground state wave function by $^{11}\text{Li}_{\text{g.s.}}$, which decays into different ^{11}Be states. The $^{11}\text{Li}_{\text{g.s.}}$ state will be constructed as a ^9Li core in its ground state, $^9\text{Li}_{\text{g.s.}}$, and two halo neutrons.

For ^{11}Be we shall consider as well the case of a two-neutron halo system having ^9Be in its ground state, $^9\text{Be}_{\text{g.s.}}$, as core. We shall denote this state as $^{11}\text{Be}_{\text{g.s.}}$. Together with it, we shall consider as well transitions into the IAS of $^{11}\text{Li}_{\text{g.s.}}$, denoted as $^{11}\text{Be}_{\text{IAS}}$, and into the AAS of $^{11}\text{Li}_{\text{g.s.}}$, denoted as $^{11}\text{Be}_{\text{AAS}}$.

It is important to note again that β decay does not change the spatial structure of the system. Therefore, all the three ^{11}Be states considered here, $^{11}\text{Be}_{\text{g.s.}}$, $^{11}\text{Be}_{\text{IAS}}$, and $^{11}\text{Be}_{\text{AAS}}$, are assumed to have the same partial wave structure (s, p, and d partial wave components) as $^{11}\text{Li}_{\text{g.s.}}$, and they all have spin and parity $3/2^-$ (so, in contrast to $^{11}\text{Li}_{\text{g.s.}}$, $^{11}\text{Be}_{\text{g.s.}}$ is not the ground state of ^{11}Be, and the subscript refers only to having ^9Be in its ground state as core).

It should be noted from the outset that our calculations will not currently be able to describe all of the decay. The decay of the core, $^9\text{Li}_{\text{g.s.}}$, proceeds about half of the time to $^9\text{Be}_{\text{g.s.}}$, and the rest of the time to excited states that are typically thought of as $^8\text{Be} +n$ and $^5\text{He} +\alpha$ combinations before decaying into a final $\alpha\alpha n$ continuum. Three-body calculations of the resonances in ^9Be are doable [17], but extending them to five-body calculations by adding two nucleons is beyond current capabilities.

Since β decay does not change the spatial wave function, the main strength will, if we neglect the small change in Coulomb energy, go to states with similar energy, and for the Fermi strength even the same energy. For ^{11}Li this implies that most strength should lie within about 5 MeV of the IAS, as the Gamow-Teller giant resonance, that includes most of the GT strength, is roughly at the IAS energy in this region of the nuclear chart [18]. This is an excitation energy where many channels are open and continuum degrees of freedom are therefore important.

For the halo decay, the GT sum rule gives a total strength of 6. The ^{11}Li halo consists mainly of $s_{1/2}^2$ and $p_{1/2}^2$ configurations. In a halo decay one of these neutrons is transformed into a proton; in most cases the ensuing configuration will not differ much in energy (and could be treated in few-body models), the main exception being for a final $p_{3/2}$ proton that could combine with the ^9Li core to produce states in ^{10}Be. The remaining $p_{1/2}$ neutron may then combine to form low-lying states in ^{11}Be, a prime example being the first excited $1/2^-$ state [19]. β transitions of this type (moving a halo particle into the core) cannot easily be reproduced in our few-body calculations.

For core decays, transitions that involve the $^9\text{Be}_{\text{IAS}}$ are straightforward to treat theoretically, even though $^9\text{Be}_{\text{IAS}}$ is inaccessible in the ^9Li decay. For all other states fed in ^9Be one has to treat them individually, find their interactions with

the halo neutrons, and extract the relevant ^9Li to $^9\text{Be}^*$ matrix elements either from experiment or from other theoretical models. We shall attempt this for the ^9Be ground state, but will not be able to treat other states. The consequences of this will be discussed in Sec. VII, as will the extent to which the ^{11}Li strength resembles the ^9Li strength.

B. The isospin wave functions

From Eq. (2) we can get the isospin wave functions for $^{11}\text{Li}_{\text{g.s.}}$ and $^{11}\text{Be}_{\text{g.s.}}$, which are given by

$$
\begin{aligned}
\left|^{11}\text{Li}_{\text{g.s.}}\right\rangle &= \left|(t_2, t_3)t_h = 1, t_c = \tfrac{3}{2}; T = \tfrac{5}{2}, T_z = -\tfrac{5}{2}\right\rangle \\
&= \left|t_c = \tfrac{3}{2} t_c^z = -\tfrac{3}{2}\right\rangle\left|t_h = 1, t_h^z = -1\right\rangle \\
&\equiv \left|^9\text{Li}_{\text{g.s.}} +n+n\right\rangle
\end{aligned}
\tag{26}
$$

and

$$
\begin{aligned}
\left|^{11}\text{Be}_{\text{g.s.}}\right\rangle &= \left|(t_2, t_3)t_h = 1, t_c = \tfrac{1}{2}; T = \tfrac{3}{2}, T_z = -\tfrac{3}{2}\right\rangle \\
&= \left|t_c = \tfrac{1}{2} t_c^z = -\tfrac{1}{2}\right\rangle\left|t_h = 1, t_h^z = -1\right\rangle \\
&\equiv \left|^9\text{Be}_{\text{g.s.}} +n+n\right\rangle,
\end{aligned}
\tag{27}
$$

where the core states $|t_c = \tfrac{3}{2}, t_c^z = -\tfrac{3}{2}\rangle$ and $|t_c = \tfrac{1}{2}, t_c^z = -\tfrac{1}{2}\rangle$ correspond to $^9\text{Li}_{\text{g.s.}}$ and $^9\text{Be}_{\text{g.s.}}$, respectively. Therefore, $^{11}\text{Li}_{\text{g.s.}}$ and $^{11}\text{Be}_{\text{g.s.}}$ correspond to three-body structures having either $^9\text{Li}_{\text{g.s.}}$ or $^9\text{Be}_{\text{g.s.}}$ as core, surrounded by two neutrons (since $t_h^z = -1$, the halo is necessarily formed by two neutrons).

Similarly, for $^{11}\text{Be}_{\text{IAS}}$ and $^{11}\text{Be}_{\text{AAS}}$, making use of Eqs. (3) and (4), we get

$$
\begin{aligned}
\left|^{11}\text{Be}_{\text{IAS}}\right\rangle &= \left|(t_2, t_3)t_h = 1, t_c = \tfrac{3}{2}; T = \tfrac{5}{2}, T_z = -\tfrac{3}{2}\right\rangle \\
&= \sqrt{\tfrac{2}{5}}\left|t_c = \tfrac{3}{2} t_c^z = -\tfrac{3}{2}\right\rangle\left|t_h = 1, t_h^z = 0\right\rangle \\
&\quad + \sqrt{\tfrac{3}{5}}\left|t_c = \tfrac{3}{2} t_c^z = -\tfrac{1}{2}\right\rangle\left|t_h = 1, t_h^z = -1\right\rangle \\
&\equiv \sqrt{\tfrac{2}{5}}\left|^9\text{Li}_{\text{g.s.}} +n+p\right\rangle + \sqrt{\tfrac{3}{5}}\left|^9\text{Be}_{\text{IAS}} +n+n\right\rangle
\end{aligned}
\tag{28}
$$

and

$$
\begin{aligned}
\left|^{11}\text{Be}_{\text{AAS}}\right\rangle &= \left|(t_2, t_3)t_h = 1, t_c = \tfrac{3}{2}; T = \tfrac{3}{2}, T_z = -\tfrac{3}{2}\right\rangle \\
&= \sqrt{\tfrac{3}{5}}\left|t_c = \tfrac{3}{2} t_c^z = -\tfrac{3}{2}\right\rangle\left|t_h = 1, t_h^z = 0\right\rangle \\
&\quad - \sqrt{\tfrac{2}{5}}\left|t_c = \tfrac{3}{2} t_c^z = -\tfrac{1}{2}\right\rangle\left|t_h = 1, t_h^z = -1\right\rangle \\
&\equiv \sqrt{\tfrac{3}{5}}\left|^9\text{Li}_{\text{g.s.}} +n+p\right\rangle - \sqrt{\tfrac{2}{5}}\left|^9\text{Be}_{\text{IAS}} +n+n\right\rangle,
\end{aligned}
\tag{29}
$$

where, as before, $|t_c = \tfrac{3}{2}, t_c^z = -\tfrac{3}{2}\rangle$ corresponds to $^9\text{Li}_{\text{g.s.}}$, but $|t_c = \tfrac{3}{2}, t_c^z = -\tfrac{1}{2}\rangle$ corresponds to ^9Be populating the IAS of $^9\text{Li}_{\text{g.s.}}$, i.e., $^9\text{Be}_{\text{IAS}}$. Therefore, both $^{11}\text{Be}_{\text{IAS}}$ and $^{11}\text{Be}_{\text{AAS}}$ mix two different three-body structures, one having $^9\text{Li}_{\text{g.s.}}$ as core, plus one neutron and one proton (as it corresponds to $t_h^z = 0$), and a second system having $^9\text{Be}_{\text{IAS}}$ as core, plus two neutrons.

As expected, the weights are such that the IAS and AAS described in Eqs. (28) and (29) are orthogonal.

Note that for all the three-body systems considered here, $^{11}\text{Li}_{\text{g.s.}}$, $^{11}\text{Be}_{\text{g.s.}}$, $^{11}\text{Be}_{\text{IAS}}$, and $^{11}\text{Be}_{\text{AAS}}$, the two halo nucleons couple to $t_h = 1$. This means that the isospin function is always symmetric under exchange of both nucleons, and therefore the three-body wave function describing the relative motion between the three constituents, Ψ_{3b}, has to be in all the cases antisymmetric under the same exchange.

C. Potential matrix elements

As mentioned, in order to obtain the three-body wave functions, it is always necessary, at some point, to compute the matrix elements $\langle \mathcal{Y}_q; T, T_z | V_{cN}^{(t_{cN})} | \mathcal{Y}_{q'}; T, T_z \rangle$, Eq. (13), which involve the different core-nucleon interactions and the basis terms formed by the usual hyperspherical harmonics, $\mathcal{Y}_q$, and the isospin function of the system, $|T T_z\rangle$. These matrix elements are, in general, computed numerically, and, as shown in Eq. (14), they permit one to determine the two-body potentials needed in order to perform the calculation.

The particularization of the potential matrix elements for the systems considered in this work, $^{11}\text{Li}_{\text{g.s.}}$, $^{11}\text{Be}_{\text{g.s.}}$, $^{11}\text{Be}_{\text{IAS}}$, and $^{11}\text{Be}_{\text{AAS}}$, can be made by use of the isospin wave functions given in Eqs. (26) to (29). The details are given in Appendix B.

In particular, from Eqs. (B9) to (B12) we get that, in order to obtain the three-body wave functions for the $^{11}\text{Li}_{\text{g.s.}}$, $^{11}\text{Be}_{\text{g.s.}}$, $^{11}\text{Be}_{\text{IAS}}$, and $^{11}\text{Be}_{\text{AAS}}$ states, the following core-nucleon interactions need to be specified: (*i*) The interaction between the $^9\text{Li}_{\text{g.s.}}$ core and the neutron (only $t_{cN} = 2$ is possible), (*ii*) the interaction between the $^9\text{Be}_{\text{g.s.}}$ core and the neutron (only $t_{cN} = 1$ is possible), (*iii*) the interaction between the $^9\text{Li}_{\text{g.s.}}$ core and the proton for $t_{cN} = 2$, (*iv*) the interaction between the $^9\text{Be}_{\text{IAS}}$ core and the neutron for $t_{cN} = 2$, (*v*) the interaction between the $^9\text{Li}_{\text{g.s.}}$ core and the proton for $t_{cN} = 1$, and (*vi*) the interaction between the $^9\text{Be}_{\text{IAS}}$ core and the neutron for $t_{cN} = 1$.

D. Core energy

In Sec. III B we described how the core Hamiltonian, $\mathcal{H}_{\text{core}}$, gives rise to a shift of the effective three-body potentials determining the energy of the different three-body states. This shift is governed by the energy of the core, which, as we can see from Eqs. (26) to (29), for the systems considered here can be either $^9\text{Li}_{\text{g.s.}}$, $^9\text{Be}_{\text{g.s.}}$, or $^9\text{Be}_{\text{IAS}}$, whose respective energies will be denoted by $\xi_{^9\text{Li}_{\text{g.s.}}}$, $\xi_{^9\text{Be}_{\text{g.s.}}}$, and $\xi_{^9\text{Be}_{\text{IAS}}}$.

The details of the calculation of these core matrix elements are given in Appendix C, and, more specifically, the shift of the effective three-body potentials is given by Eqs. (C4) to (C7).

E. Relative energies

In this work we are describing four different three-body systems, i.e., $^{11}\text{Li}_{\text{g.s.}}$, $^{11}\text{Be}_{\text{g.s.}}$, $^{11}\text{Be}_{\text{IAS}}$, and $^{11}\text{Be}_{\text{AAS}}$. When computed individually, it is common to refer the energy of the three-body states to three-body thresholds. In other words, the

zero-energy point is taken as the energy of the core for each of them.

However, in order to describe the decay of some system ($^{11}\text{Li}_{\text{g.s.}}$ in our case) into some other systems (three different ^{11}Be states in our calculations) it is necessary to refer all the energies to a single zero-energy value. In our calculations we have chosen the zero-energy point as the $^{11}\text{Li}_{\text{g.s.}}$ threshold, which implies that $\xi_{^9\text{Li}_{\text{g.s.}}} = 0$ in Eq. (C1). After this choice, as one can find in [20], we have that $\xi_{^9\text{Be}_{\text{g.s.}}} = -13.6067$ MeV and $\xi_{^9\text{Be}_{\text{IAS}}} = 0.7855$ MeV.

The relative energies between the different systems involved in our calculations are sketched in Fig. 1 (data from Ref. [20]). The values of $\xi_{^9\text{Be}_{\text{g.s.}}}$ and $\xi_{^9\text{Be}_{\text{IAS}}}$ given above amount to an excitation energy of 14.3922 MeV of $^9\text{Be}_{\text{IAS}}$ with respect to $^9\text{Be}_{\text{g.s.}}$, which in turn is 6.8122 MeV above the ^{10}Be ground state energy. This leads to an energy threshold of 21.2044 MeV for the $^9\text{Be}_{\text{IAS}}$ +neutron state above the ^{10}Be ground state. Also, the experimental excitation energy of $^{11}\text{Be}_{\text{IAS}}$ with respect to $^{11}\text{Be}_{\text{g.s.}}$, 21.16 MeV, gives rise to an excitation energy of only 0.24 MeV with respect to the $^{11}\text{Li}_{\text{g.s.}}$ threshold.

V. THREE-BODY CALCULATIONS

In order to perform the three-body calculations, the key quantities are the two-body interactions between the three constituents of the systems. We now describe how these interactions are constructed, and discuss the three-body wave functions obtained after the subsequent calculations.

A. Two-body potentials

The systems involved in this work are $^{11}\text{Li}_{\text{g.s.}}$, $^{11}\text{Be}_{\text{g.s.}}$, $^{11}\text{Be}_{\text{IAS}}$, or $^{11}\text{Be}_{\text{AAS}}$. The required core-nucleon interactions are the six interactions mentioned in Sec. IV C, which, together with the nucleon-nucleon potential, constitute all the interactions needed for the calculations.

For the nucleon-nucleon interaction we use the potential given in Eq. (5) of Ref. [21]. This is a simple potential employing Gaussian shapes for the central, spin-spin, spin-orbit, and tensor terms, and whose parameters (strength and range) are adjusted to reproduce the experimental s- and p-wave nucleon-nucleon scattering lengths and effective ranges.

For all the necessary core-nucleon interactions we take an ℓ dependent potential with the form

$$V_{cN}^{(\ell)}(r) = V_c^{(\ell)}(r) + V_{ss}^{(\ell)}(r)\boldsymbol{s}_c \cdot \boldsymbol{j}_N + V_{so}^{(\ell)}(r)\boldsymbol{\ell} \cdot \boldsymbol{s}_N, \quad (30)$$

with central, spin-spin, and spin-orbit terms (plus Coulomb interaction when needed). In the expression above, $\boldsymbol{s}_c$ and $\boldsymbol{s}_N$ are the spins of the core and the nucleon, respectively, $\boldsymbol{\ell}$ is the relative orbital angular momentum between them, and $\boldsymbol{j}_N$ results from the coupling of $\boldsymbol{\ell}$ and $\boldsymbol{s}_N$. This choice of the spin-spin and spin-orbit operators is particularly useful to preserve the shell-model quantum numbers for the nucleon state, making easier the implementation of the Pauli principle [22]. In all the cases the potential functions $V_c^{(\ell)}$, $V_{ss}^{(\ell)}$, and $V_{so}^{(\ell)}$ are taken to be Gaussians whose parameters are adjusted to reproduce the available experimental information about the core-nucleon system.
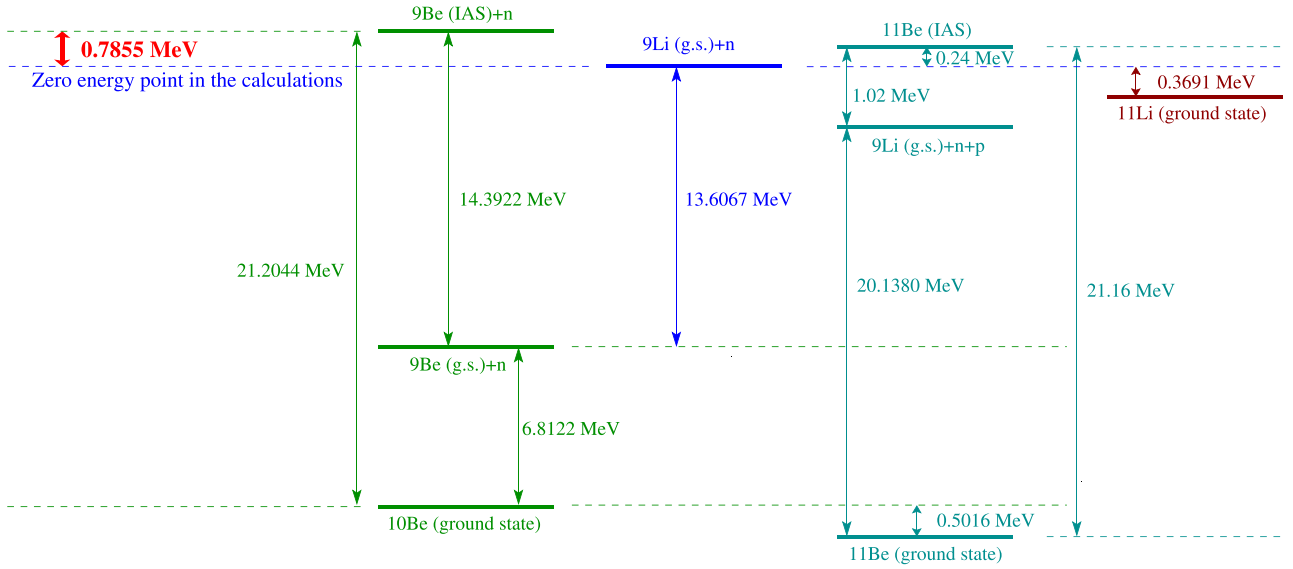
FIG. 1. Relative energies between the different states involved in the calculations. Data are from Ref. [20]. To keep the figure clean, the separation between the states is not always properly scaled.

The connection to an explicit isospin dependence is described in Appendix A, where the expression of the potential can be found for use if the isospin formalism is preferred.

Below we describe how the different potentials, (*i*), (*ii*), (*iii*), (*iv*), (*v*), and (*vi*), as labeled in Sec. IV C, are selected.

(*i*) and (*iii*): For the neutron-^{9}Li$_{g.s.}$ interaction [potential (*i*)], which enters in the matrix elements (B9), (B11), and (B12), we use the interaction specified in Ref. [13] to describe the ^{11}Li ground state. The given Gaussian potentials are shallow enough to avoid binding of a halo nucleon into a Pauli forbidden state. In particular, since the $p_{3/2}$ shell is fully occupied by the neutrons in the core, the p-wave spin-orbit potential is used to push the $p_{3/2}$ states away. As shown in Eq. (B1), the neutron-^{9}Li$_{g.s.}$ interaction corresponds fully to a core-neutron isospin $t_{cN} = 2$. The precise parameters of the potential for s, p, and d waves are given in the second column of Table I. The same interaction is used for the proton-^{9}Li$_{g.s.}$ potential with $t_{cN} = 2$ [potential (*iii*)], entering in the matrix

elements (B11) and (B12), simply by adding the corresponding core-proton Coulomb repulsion.

(*ii*): For the neutron-^{9}Be$_{g.s.}$ interaction the potential is fitted to reproduce the known ^{10}Be properties [20]. The ^{9}Be core has spin and parity $J^\pi = \frac{3}{2}^-$, which, when coupled to an $s_{1/2}$ neutron, gives rise to a 1^- and a 2^- state. Experimentally, ^{10}Be is known to have such a 1^- and 2^- states, both bound with respect to the ^{9}Be-neutron threshold by 0.8523 and 0.5489 MeV, respectively. These two states are then used to construct the s-wave potential. In the same way the 2^+ state, bound by 0.8538 MeV, is used to obtain the p-wave potential. Experimentally, there is no low-lying 1^+ state, and the spin-spin interaction is then used to push away this state. Also, since the partial wave structure of the system is the same as the one in ^{11}Li$_{g.s.}$, the spin-orbit potential is employed to move away the Pauli forbidden $p_{3/2}$ states. Finally, the 4^- and 3^- states, with excitation energies 9.27 and 10.15 MeV, respectively, are used to estimate the potential parameter for d waves. This interaction enters in the matrix element (B10) only, and it corresponds to $t_{cN} = 1$. The parameters of the neutron-^{9}Be$_{g.s.}$ potential are given in the fourth column of Table I.

(*iv*): For the neutron-^{9}Be$_{IAS}$ interaction and $t_{cN} = 2$ we take into account that ^{9}Be$_{IAS}$ is the IAS of the ^{9}Li$_{g.s.}$. The members of a given isobaric multiplet preserve the nuclear structure, in such a way that the energy difference between them is provided almost exclusively by the different strength of the Coulomb repulsion. For this reason, when $t_{cN} = 2$, we use for the neutron-^{9}Be$_{IAS}$ interaction, which enters in the matrix elements (B11) and (B12), the same nuclear potential as for the neutron-^{9}Li$_{g.s.}$ interaction, which is given in the second column of Table I.

(*v*) and (*vi*): For the proton-^{9}Li$_{g.s.}$ and neutron-^{9}Be$_{IAS}$ potentials with $t_{cN} = 1$, since, as mentioned above, the ^{9}Li$_{g.s.}$ and ^{9}Be$_{IAS}$ cores belong to the same isospin multiplet, we take in

TABLE I. Strengths, in MeV, of the nuclear Gaussian potentials $[V^{(\ell)}(r) = S^{(\ell)}e^{-r^2/b^2}]$ for the six potentials, labeled as in Sec. IV C, entering in this work. The range of the Gaussians is $b = 3.0$ fm for potential (*ii*) and $b = 2.55$ fm for the other five potentials.

	$t_{cN} = 2$	$t_{cN} = 1$	n-^{9}Be$_{g.s.}$
Pots.	(*i*), (*iii*), (*iv*)	(*v*), (*vi*)	(*ii*)
$S_c^{(s)}$	−5.4	−23.61	−11.47
$S_c^{(p)}$	260.75	246.70	−1.89
$S_c^{(d)}$	260	246.70	−44.22
$S_{ss}^{(s)}$	−4.5w	−1.83	0.59
$S_{ss}^{(p)}$	1.0	−3.35	−4.0
$S_{ss}^{(d)}$	−9.0	−3.35	−0.88
$S_{so}^{(p)}$	300	300	30.0
$S_{so}^{(d)}$	−300	−300	−10.0

both cases the same nuclear potential. The Coulomb repulsion is the only difference between both interactions.

For the case of the $^9\text{Be}_{\text{IAS}}$ +neutron system, the $t_{cN} = 1$ states are the antianalog states of the ^{10}Li low-lying states, whose energy is about 20 MeV above the ^{10}Be ground state, as shown in Fig. 1. Similar pairs of known IAS-AAS partners suggest that the antianalog states lie a few MeV below the isobaric analog states. Therefore, the $^9\text{Be}_{\text{IAS}}$ +neutron ($t_{cN} = 1$) states are expected to be located about 16 to 18 MeV above the ^{10}Be ground state. Good candidates are therefore the experimentally known ^{10}Be states with excitation energies 17.12, 17.79, and 18.55 MeV [20]. This is actually supported by the fact that, for the $^9\text{Be}_{\text{IAS}}$ +proton (^{10}B) system, which except for the Coulomb repulsion is equivalent to the $^9\text{Be}_{\text{IAS}}$ +neutron system, there is a known series of isospin 1 states at an energy of about 18 MeV above the ^{10}Be ground state, among which a 2^-, a 2^+, and a 1^- state have been observed.

For this reason we have assumed that the first and third of the mentioned ^{10}Be states, at 17.12 and 18.55 MeV, are 2^- and 1^- states arising from the coupling of an $s_{1/2}$ neutron and the core ($J^\pi = \frac{3}{2}^-$), and the second state, at 17.79 MeV, is assumed to be a 2^+ state coming from the coupling of a $p_{1/2}$ neutron and the core. As in the neutron-$^9\text{Li}_{\text{g.s.}}$ interaction, the $p_{3/2}$ neutron states are pushed away. The precise parameters are given in the third column of Table I. For the d waves we use the same potential as for the p waves but changing the sign in the spin-orbit potential (as systematically happens for the other potentials). At this point it is important to keep in mind the relative energies between all the systems involved in our calculations, which are shown in Fig. 1. The 2^-, 2^+, and 1^- states in ^{10}Be used to determine the $t_{cN} = 1$ part of the interaction, with excitation energies all around 18 MeV above the ^{10}Be ground state, are actually below the $^9\text{Be}_{\text{IAS}}$-neutron threshold, and therefore they are bound with respect to this threshold by 4.08, 3.41, and 2.65 MeV, respectively.

An additional simplification comes from treating the $^9\text{Be}_{\text{IAS}}$ core as a single particle; $^9\text{Be}_{\text{IAS}}$ is far from being bound, although it is quite narrow (less than one keV). One could envisage describing the $^9\text{Be}_{\text{IAS}}$ +neutron system as a four-body ($\alpha + \alpha + n + n$) system, and consequently the corresponding ^{11}Be states as a five-body system. In any case this is out of our reach, as it would make the calculations significantly more complex.

B. Three-body wave functions

Using the interactions as described above, we have made the three-body calculations for $^{11}\text{Li}_{\text{g.s.}}$, $^{11}\text{Be}_{\text{g.s.}}$, $^{11}\text{Be}_{\text{IAS}}$, and $^{11}\text{Be}_{\text{AAS}}$. Among them the more tricky ones are the calculations of $^{11}\text{Be}_{\text{IAS}}$ and $^{11}\text{Be}_{\text{AAS}}$, since, as shown in Eqs. (B11) and (B12), they both combine different core-nucleon potentials, and, in the case of $^{11}\text{Be}_{\text{AAS}}$, also different values of t_{cN}.

In Fig. 2(a) we show for these two systems the four lowest computed effective adiabatic potentials as defined in Eq. (6). The solid-red and dashed-green curves correspond, respectively, to the $^{11}\text{Be}_{\text{IAS}}$ and the $^{11}\text{Be}_{\text{AAS}}$ systems. We can immediately see that the potentials for the AAS are clearly deeper than the ones for the IAS. This is expected, since in the AAS case the interaction contains the $t_{cN} = 1$ part of
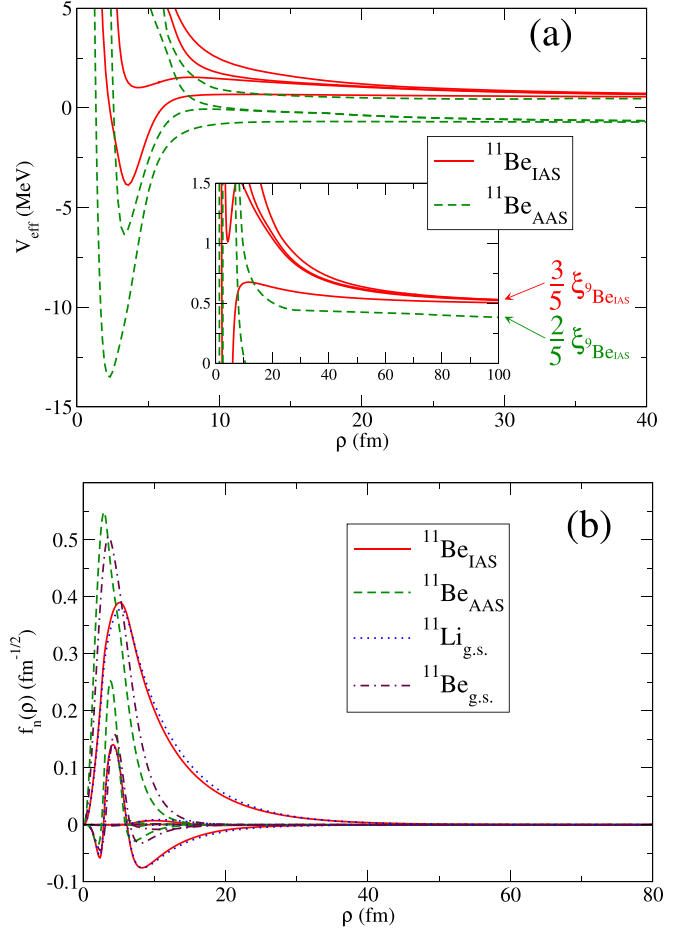

FIG. 2. (a) The four lowest effective potentials for the IAS (solid red) and AAS (dashed green) in ^{11}Be. The inset shows a zoom of the large distance behavior. (b) Radial wave functions for the four lowest adiabatic terms for $^{11}\text{Be}_{\text{IAS}}$ (solid red), $^{11}\text{Be}_{\text{AAS}}$ (dashed green), $^{11}\text{Li}_{\text{g.s.}}$ (dotted blue), and $^{11}\text{Be}_{\text{g.s.}}$ (dot-dashed brown).

the potential, which, as explained above, binds by several MeV the lowest 2^-, 1^-, and 2^+ states in the $^9\text{Be}_{\text{IAS}}$-neutron system with respect to the $^9\text{Be}_{\text{IAS}}$-neutron threshold. In fact, the lowest AAS potentials go asymptotically to the energies of the bound $^9\text{Be}_{\text{IAS}}$-neutron states, although weighted with the geometric factors involved in the matrix element in Eq. (B8).

The higher potentials in the AAS case, as well as the ones for the IAS, go asymptotically to the value determined by the energy shift imposed by the core Hamiltonian in Eqs. (C6) and (C7), i.e., $\frac{3}{5}\xi_{^9\text{Be}_{\text{IAS}}}$ and $\frac{2}{5}\xi_{^9\text{Be}_{\text{IAS}}}$ for the IAS and AAS, respectively, where $\xi_{^9\text{Be}_{\text{IAS}}} = 0.7855$ MeV (see Fig. 1). This is seen in the inset in Fig. 2(a), which shows the large distance part of the potentials.

As shown in Fig. 1, the experimental excitation energy of $^{11}\text{Be}_{\text{IAS}}$ is 21.16 MeV, which is 0.24 MeV above the $^9\text{Li}_{\text{g.s.}} + n + n$ threshold that we take as our zero-energy point. This value of the IAS energy, 0.24 MeV, is below the asymptotic energy limit, $\frac{3}{5}\xi_{^9\text{Be}_{\text{IAS}}} = 0.47$ MeV, of the potentials shown in the inner panel in Fig. 2(a), which implies that the computed radial wave function will decay exponentially at large distances, as a regular bound state. The same of course

TABLE II. Computed excitation energies (second column) and energies relative to the ^{9}Li$_{g.s.}$ $+n+n$ threshold (third column) for ^{11}Li$_{g.s.}$, ^{11}Be$_{g.s.}$, ^{11}Be$_{IAS}$, and ^{11}Be$_{AAS}$. All energies are given in MeV.

	Excitation energy	^{9}Li$_{g.s.}$ $+n+n$
^{11}Li$_{g.s.}$	0	-0.37
^{11}Be$_{g.s.}$	2.89	-18.03
^{11}Be$_{IAS}$	21.16	0.24
^{11}Be$_{AAS}$	15.39	-5.53

happens for the AAS, which, as one can anticipate from Fig. 2(a), is going to be clearly more bound than the IAS.

In the calculation for ^{11}Li$_{g.s.}$ and ^{11}Be$_{IAS}$ it has been necessary to introduce a small attractive effective three-body force in such a way that the respective experimental energies, -0.369 and 0.24 MeV with respect to the energy threshold shown in Fig. 1, are well reproduced. For ^{11}Be$_{AAS}$ the same effective three-body force as for the IAS has been used, and a binding energy of -5.53 MeV with respect to our zero energy point has been obtained. This amounts to an excitation energy of this ^{11}Be state of 15.39 MeV, which is consistent with observations in other IAS/AAS partners. Also, the computed energy difference between the IAS and AAS is equal to 5.77 MeV, consistent as well with the upper limit of 7 MeV estimated in Appendix A.

Finally, for ^{11}Be$_{g.s.}$ the three-body calculation without any three-body potential gives rise to a binding energy of -18.03 MeV with respect to our chosen zero-energy value. This means, see Fig. 1, that the computed ^{11}Be$_{g.s.}$ wave function has an excitation energy of 2.89 MeV with respect to the ground state of ^{11}Be. Since this excitation energy is in the vicinity of the experimentally known $3/2^-$ states in ^{11}Be with excitation energy 2.69 MeV and 3.97 MeV, we then have not included any three-body potential for ^{11}Be$_{g.s.}$.

The computed energies for ^{11}Li$_{g.s.}$, ^{11}Be$_{g.s.}$, ^{11}Be$_{IAS}$, and ^{11}Be$_{AAS}$ are summarized in Table II, where the second column gives the excitation energies and the third one the same energies but relative to the ^{9}Li$_{g.s.}$ $+n+n$ threshold used in this work. All the energies are given in MeV.

In Fig. 2(b) we plot the radial wave functions associated to the four lowest adiabatic terms, Eq. (5), for each of the systems computed in this work, i.e., ^{11}Be$_{IAS}$ (solid red), ^{11}Be$_{AAS}$ (dashed green), ^{11}Li$_{g.s.}$ (dotted blue), and ^{11}Be$_{g.s.}$ (dot-dashed brown). As we can see, in all the cases the first two terms provide almost the full wave function. The wave functions for ^{11}Be$_{IAS}$ and ^{11}Li$_{g.s.}$ are very similar. This is due to the fact that in both cases only the $t_{CN} = 2$ part of the core-nucleon potential enters. Since the cores in both systems belong to the same isospin multiplet the nuclear interaction is therefore the same for the two of them. The only difference comes from the Coulomb repulsion present in the ^{9}Li$_{g.s.}$ $+n+p$ structure entering in the IAS case; see Eq. (28).

VI. β DECAY STRENGTH

The energy distribution for a β decay transition is given by Eq. (24). The initial state is ^{11}Li$_{g.s.}$, whose isospin wave
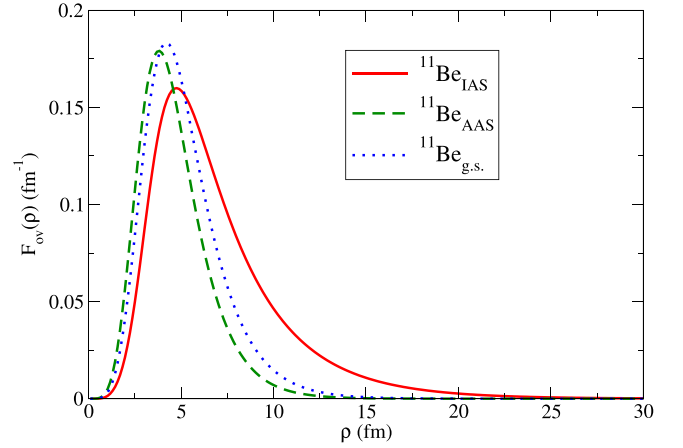

FIG. 3. $F_{ov}(\rho)$ function in Eq. (31) for the overlap between the ^{11}Li$_{g.s.}$ wave function and the one corresponding to ^{11}Be$_{IAS}$ (solid), ^{11}Be$_{AAS}$ (dashed), and ^{11}Be$_{g.s.}$ (dotted).

function is given by Eq. (26). For the final states we consider either ^{11}Be$_{g.s.}$, Eq. (27), ^{11}Be$_{IAS}$, Eq. (28), or ^{11}Be$_{AAS}$, Eq. (29).

A. Overlap between initial and final wave functions

One of the ingredients that enter in both, Fermi and Gamow-Teller, transition strengths is the overlap between the initial and final three-body wave functions (excluding the isospin part), $\Psi_{3b}^{(in)}$ and $\Psi_{3b}^{(fin)}$. In order to investigate this overlap, we introduce the overlap function

$$F_{ov}(\rho) = \int \rho^5 \Psi_{3b}^{(fin)}(\rho, \Omega) \Psi_{3b}^{(in)}(\rho, \Omega) d\Omega, \qquad (31)$$

where the integral is over the five hyperangles only. With this definition we have that

$$\int d\rho F_{ov}(\rho) = \langle \Psi_{3b}^{(fin)} | \Psi_{3b}^{(in)} \rangle = \frac{1}{\sqrt{2J_i + 1}} \langle \Psi_{3b}^{(fin)} || \Psi_{3b}^{(in)} \rangle. \qquad (32)$$

In Fig. 3 we show the overlap function in Eq. (31), where $\Psi_{3b}^{(in)}$ is the wave function of ^{11}Li$_{g.s.}$ and $\Psi_{3b}^{(fin)}$ is the wave function of either ^{11}Be$_{IAS}$ (solid curve), ^{11}Be$_{AAS}$ (dashed curve), or ^{11}Be$_{g.s.}$ (dotted curve). Due to the similarity between the ^{11}Li$_{g.s.}$ and ^{11}Be$_{IAS}$ wave functions, dotted and solid curves in Fig. 2(b), the integral over ρ, Eq. (32), of the corresponding overlap function (solid curve in Fig. 3) is 0.99, very close to 1. As we can also anticipate from Fig. 2(b), the cases of ^{11}Be$_{AAS}$ and ^{11}Be$_{g.s.}$ are different. These wave functions are clearly narrower than the one of ^{11}Li$_{g.s.}$, and, as a consequence, the integral over ρ of the overlap function (dashed and dotted curves in Fig. 3) will be significantly smaller, 0.72 and 0.82 for ^{11}Be$_{AAS}$ and ^{11}Li$_{g.s.}$, respectively.

At this point it is interesting to introduce the effect of the continuum background in the overlap functions by means of the differential distribution

$$\frac{dB_{ov}}{dE} = \frac{1}{2J_i + 1} \sum_k \delta(E - E_k) |\langle \Psi_{3b}^{(fin)}(E_k) || \Psi_{3b}^{(in)} \rangle|^2, \qquad (33)$$
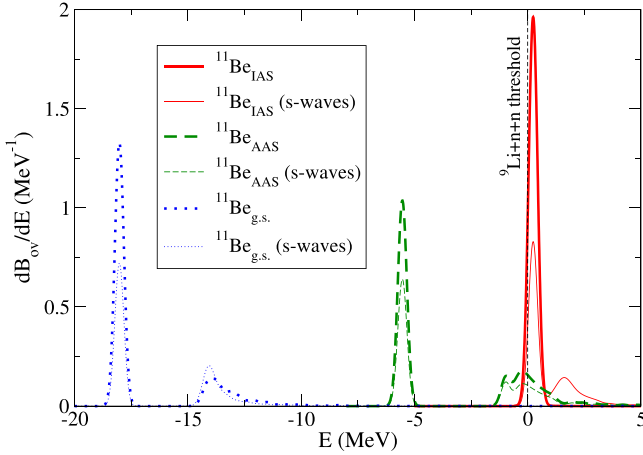
FIG. 4. Overlap strength, as given in Eq. (33), as a function of the three-body energy, for transitions into states, bound and continuum, with the same quantum numbers as ^{11}Be$_{\rm IAS}$ (solid red), ^{11}Be$_{\rm AAS}$ (dashed green), and ^{11}Be$_{\rm g.s.}$ (dotted blue). The thin curves show the contribution from core-nucleon s waves only.

which is analogous to the differential transition strength introduced in Eq. (24), and where k runs over all the discretized continuum states.

The result from Eq. (33) is shown in Fig. 4 for transitions into states, bound and continuum, with the same quantum numbers, as ^{11}Be$_{\rm IAS}$ (solid red), ^{11}Be$_{\rm AAS}$ (dashed green), and ^{11}Be$_{\rm g.s.}$ (dotted blue). The thin curves in the figure give the contribution when only the relative core-nucleon s waves are considered. The three main peaks are produced by the transitions into the specific ^{11}Be$_{\rm IAS}$, ^{11}Be$_{\rm AAS}$, and ^{11}Be$_{\rm g.s.}$ states, which provide most of the contribution to $B_{\rm ov}$. The remainder is the contribution from the continuum states. We can see there is a non-negligible contribution from the continuum states for transitions into the states with the ^{11}Be$_{\rm AAS}$ and ^{11}Be$_{\rm g.s.}$ quantum numbers. For the ^{11}Be$_{\rm IAS}$, the s-wave contribution (thin solid) has a bump at about 2 MeV, but this bump disappears from the total due to the interference with the other partial waves, in such a way that the contribution from the continuum states is negligible.

The integral over E of the different curves in Fig. 4 gives the total value, $B_{\rm ov}$, of the overlap, which is 0.99, 0.87, and 0.90 for states with the same quantum numbers as ^{11}Be$_{\rm IAS}$, ^{11}Be$_{\rm AAS}$, and ^{11}Be$_{\rm g.s.}$, respectively. The total contribution from the specific ^{11}Be$_{\rm IAS}$, ^{11}Be$_{\rm AAS}$, and ^{11}Be$_{\rm g.s.}$ states is given by the square of Eq. (32), which, as obtained after the analysis of Fig. 3, is equal to 0.98, 0.52, and 0.67 for the three cases. In other words, the contribution from the continuum background is very small (≈ 0.01) for the IAS case, but quite relevant, 0.35 and 0.23, for the other two cases. These results are summarized in the first three rows in Table III.

In the table, in the last three rows, we also give the contribution to the total when only the relative core-nucleon s waves, p waves, and d waves are included. As we can see, the contribution to the overlaps from the d waves is negligible in all the three cases. Also, the weight of s and p partial waves is similar in the three cases too, especially if we consider the

TABLE III. Integrated overlap function, $B_{\rm ov}$, from Eq. (33), for the states with same quantum numbers as ^{11}Be$_{\rm IAS}$, ^{11}Be$_{\rm AAS}$, and ^{11}Be$_{\rm g.s.}$. The following two rows give the contributions to the total from the noncontinuum states and the continuum background, respectively. The last three rows give the contribution to the total when only relative core-nucleon s waves, p waves, and d waves are included. The values within parenthesis give the percentage over the total given by each contribution.

	^{11}Be$_{\rm IAS}$	^{11}Be$_{\rm AAS}$	^{11}Be$_{\rm g.s.}$
$B_{\rm ov}$ (total)	0.99	0.87	0.90
$B_{\rm ov}$ (no cont.)	0.98 (99%)	0.52 (60%)	0.67 (74%)
$B_{\rm ov}$ (continuum)	0.01 (1%)	0.35 (40%)	0.23 (26%)
$B_{\rm ov}$ (s waves)	0.63 (64%)	0.56 (64%)	0.59 (66%)
$B_{\rm ov}$ (p waves)	0.30 (30%)	0.28 (32%)	0.23 (26%)
$B_{\rm ov}$ (d waves)	0.00 (0%)	0.00 (0%)	0.00 (0%)

percentage over the total given by each of them, which is indicated in the table within parenthesis. Note that the sum of the s, p, and d contributions does not provide the total value of $B_{\rm ov}$. The missing contribution, which ranges from 4% to 8% depending on the case, is the contribution from the s, p, and d interferences when squaring the overlap in Eq. (32), which, by construction, are omitted when the calculation is limited to s, p, or d waves.

Note as well that, although the value of the integral over E of Eq. (33) is independent of σ, see Eq. (25), the height of the peaks of the curves in Fig. 4 is very sensitive to its value. In this calculation we have taken $\sigma = 0.2$ MeV, but a value slightly smaller can produce curves with clearly higher peaks, that one could still consider smooth. Therefore, whereas the curves in Fig. 4 can be seen as an estimate of the differential overlap, the integral under the curves, the integrated strengths, Table III, which are the relevant quantities in order to obtain the total transition strengths, are well established results of the calculations.

B. Fermi decay

For Fermi transitions, the β decay matrix element is given by Eq. (23), which simply is the overlap $\langle \Psi_{3b}^{\rm (fin)} || \Psi_{3b}^{\rm (in)} \rangle$ as given in Eq. (32), multiplied by a global isospin dependent factor. Therefore, as seen from Eq. (24), the corresponding differential transition strength will be the overlap strength defined in Eq. (33), multiplied by the isospin global factor squared. In other words, the differential Fermi transition strength for the different transitions considered in this work is given by the curves in Fig. 4, but each of them has to be multiplied by the corresponding isospin factor squared.

As we can see in Eq. (23), the isospin factor contains three ingredients, $f_{\rm fin}$, the halo isospin matrix element $\langle T, T_z | \sum_{j=v_1, v_2} t_j^+ | T', T_z' \rangle$, and the core isospin matrix element $\langle t_c, t_c^z | \sum_{j \in {}^9 {\rm Li}_{\rm g.s.}} t_j^+ | t_c' = \frac{3}{2}, t_c'^z = -\frac{3}{2} \rangle$.

For the decay of ^{11}Li$_{\rm g.s.}$ into ^{11}Be$_{\rm g.s.}$, due to the different initial and final core isospins, $\frac{3}{2}$ in the case of ^{9}Li$_{\rm g.s.}$ and $\frac{1}{2}$ for ^{9}Be$_{\rm g.s.}$, both the halo isospin matrix element and the core isospin matrix element (which in this case corresponds

TABLE IV. For decays into $^{11}\text{Be}_{\text{g.s.}}$, $^{11}\text{Be}_{\text{AAS}}$, and $^{11}\text{Be}_{\text{IAS}}$, we give the values of the halo isospin matrix element (second column), f_{fin} factor (third column), and core isospin matrix element (fourth column), entering into the total isospin term (fifth column) in Eq. (23).

Daughter	$\langle \sum_{j=v_1,v_2} t_j^+ \rangle$	f_{fin}	$\langle \sum_{j\in{}^9\text{Li}_{\text{g.s.}}} t_j^+ \rangle$	Total
$^{11}\text{Be}_{\text{g.s.}}$	0	1	0	0
$^{11}\text{Be}_{\text{AAS}}$	$\sqrt{\frac{6}{5}}$	$-\sqrt{\frac{2}{5}}$	$\sqrt{3}$	0
$^{11}\text{Be}_{\text{IAS}}$	$\frac{2}{\sqrt{5}}$	$\sqrt{\frac{3}{5}}$	$\sqrt{3}$	$\sqrt{5}$

to $t_c = \frac{1}{2}$ and $t_c^z = -\frac{1}{2}$) are equal to zero. Therefore the isospin factor is in this case equal to zero, and there is no Fermi transition between $^{11}\text{Li}_{\text{g.s.}}$ and $^{11}\text{Be}_{\text{g.s.}}$. These values are collected into the second row of Table IV.

For transitions from $^{11}\text{Li}_{\text{g.s.}}$ into $^{11}\text{Be}_{\text{AAS}}$, as shown in Eq. (21) for $t_c = 3/2$ and $t_h = 1$, we have that $f_{\text{fin}} = -\sqrt{2/5}$. In this case the halo isospin matrix element takes the value $\sqrt{6/5}$, and the core isospin matrix element, with $t_c = \frac{3}{2}$ and $t_c^z = -\frac{1}{2}$, is equal to $\sqrt{3}$. When these values are combined to get the isospin factor in Eq. (23), we obtain that its value is equal to zero (third row of Table IV). The Fermi transition between $^{11}\text{Li}_{\text{g.s.}}$ and $^{11}\text{Be}_{\text{AAS}}$ is forbidden as it connects states with different T.

Finally, for transitions from $^{11}\text{Li}_{\text{g.s.}}$ into $^{11}\text{Be}_{\text{IAS}}$, Eq. (20) for $t_c = 3/2$ and $t_h = 1$ results in $f_{\text{fin}} = \sqrt{3/5}$. In this case the halo isospin matrix element is equal to $2/\sqrt{5}$, and, as for transitions into the AAS, the core isospin matrix element is $\sqrt{3}$. All this results in a global isospin term in Eq. (23) equal to $\sqrt{5}$ (again, these values are collected in Table IV, last row). Therefore, a Fermi transition between $^{11}\text{Li}_{\text{g.s.}}$ and $^{11}\text{Be}_{\text{IAS}}$ is possible, and the corresponding differential transition strength is given by the solid (red) curve in Fig. 4, but multiplied by a factor of 5. As a consequence, as $B_{\text{ov}} = 0.99$ in this case (see Table III), the total Fermi strength is also approximately equal to 5 for this transition.

As mentioned, the products of a β decay process have, in general, a non-well-defined isospin. This quantum number is not a fundamental symmetry, since the long-range Coulomb interaction breaks the symmetry. Note that isospin breaking has been found to be small in earlier explicit calculations for halo states [23,24].

Therefore, the daughter state of the $^{11}\text{Li}_{\text{g.s.}}$ nucleus could actually mix both the $^{11}\text{Be}_{\text{IAS}}$ and the $^{11}\text{Be}_{\text{AAS}}$ states. In order to estimate the isospin admixture of these states we closely follow the procedure described in [24] [more precisely, Eqs. (7) and (8) of that reference]. The matrix element between the spatial wave functions of the IAS and AAS of the Coulomb potential, $Z_c e^2/r$ (where Z_c is the ^9Li charge, $e^2 = 1.44$ MeV fm, and r is the core-proton distance) is equal to 1.31 MeV. For the Coulomb displacement of the core, ΔE_c in [24], we use the energy shift between $^9\text{Li}_{\text{g.s.}}$ and $^9\text{Be}_{\text{IAS}}$, which, as shown in Fig. 1, is equal to 0.7855 MeV. All these values, together with the overlap of the spatial IAS and AAS wave functions, gave the result 0.74, and the core

and halo isospins, t_c and t_h, leads to the expectation value $\langle H_{\text{coupl}} \rangle = 0.35$ MeV, which by means of Eq. (8) in [24], and making use of the computed energy difference between the IAS and AAS, 5.77 MeV, leads to an isospin mixing $\alpha^2 = \sin^2 \theta = 3.7 \times 10^{-3}$.

C. Gamow-Teller decay

The Gamow-Teller decay matrix element is given by Eq. (22), and it contains the summation of two terms: the matrix element of the Gamow-Teller operator involving the valence nucleons, and a term proportional to the same overlap, $\langle \Psi_{3b}^{(\text{fin})} || \Psi_{3b}^{(\text{in})} \rangle$, as the one needed for the Fermi decay, and which comes from the Gamow-Teller decay of the core. The mixing of these two terms is dictated by the factor

$$f_{\text{mix}} = f_{\text{fin}} \left\langle t_c, t_c^z \left| \sum_{j\in{}^9\text{Li}} \sigma_j t_j^+ \right| t_c' = \frac{3}{2}, t_c'^z = -\frac{3}{2} \right\rangle, \quad (34)$$

which includes the Gamow-Teller matrix element describing the decay of the $^9\text{Li}_{\text{g.s.}}$ core into a core with isospin quantum numbers t_c and t_c^z.

The first of the two terms mentioned above, the matrix element describing the Gamow-Teller decay of the valence nucleons, is zero for decays into $^{11}\text{Be}_{\text{g.s.}}$. This is due to the different core isospin in the initial ($t_c' = \frac{3}{2}$) and final ($t_c = \frac{1}{2}$) states. For decays into $^{11}\text{Be}_{\text{IAS}}$ and $^{11}\text{Be}_{\text{AAS}}$ this is no longer true, because, as seen in Eqs. (28) and (29), the wave functions for these two states have a component corresponding to a $^9\text{Li}_{\text{g.s.}}$ core plus a neutron and a proton. However, the numerical calculation of this matrix element for these two transitions gives rise to a very small number, about 10^{-3} in both cases, which permits one to predict that the contribution to the Gamow-Teller strength from the decay of one of the halo neutrons is going to be, in any case, very small. This is due to the fact that this contribution is given only by the components in the initial and final wave functions with relative nucleon-nucleon p waves and nucleon-nucleon spin equal to 1, which have a very minor weight in the wave functions.

The second term in the Gamow-Teller strength comes from β decay of the core, whose β decay transition matrix element enters in the parameter given in Eq. (34). From Eqs. (20) and (21) we see that for the decay into both $^{11}\text{Be}_{\text{IAS}}$ and $^{11}\text{Be}_{\text{AAS}}$ the core-decay matrix element describes the decay $^9\text{Li}_{\text{g.s.}}$ into the same core state, in particular the core state with $t_c = \frac{3}{2}$ and $t_c^z = -\frac{1}{2}$, which corresponds to $^9\text{Be}_{\text{IAS}}$. In the same way, for a transition into $^{11}\text{Be}_{\text{g.s.}}$, we see from Eq. (19) that $t_c = \frac{1}{2}$ and $t_c^z = -\frac{1}{2}$, and the core matrix element in Eq. (34) refers to the decay of $^9\text{Li}_{\text{g.s.}}$ into $^9\text{Be}_{\text{g.s.}}$.

Appropriate values for the core Gamow-Teller matrix elements may be estimated from shell-model calculations for the decay of $^9\text{Li}_{\text{g.s.}}$, as shown in Ref. [6]. In this work the values of 0.5 and 0.1 are given for the Gamow-Teller strength for decays of $^9\text{Li}_{\text{g.s.}}$ into $^9\text{Be}_{\text{IAS}}$ and $^9\text{Be}_{\text{g.s.}}$, respectively. The square roots of these values give then the transition matrix element entering in Eq. (34) for each case, which give rise to $f_{\text{mix}} = 0.55$, -0.45, and 0.32 for decays into $^{11}\text{Be}_{\text{IAS}}$, $^{11}\text{Be}_{\text{AAS}}$, and $^{11}\text{Be}_{\text{g.s.}}$, respectively. To get these numbers one
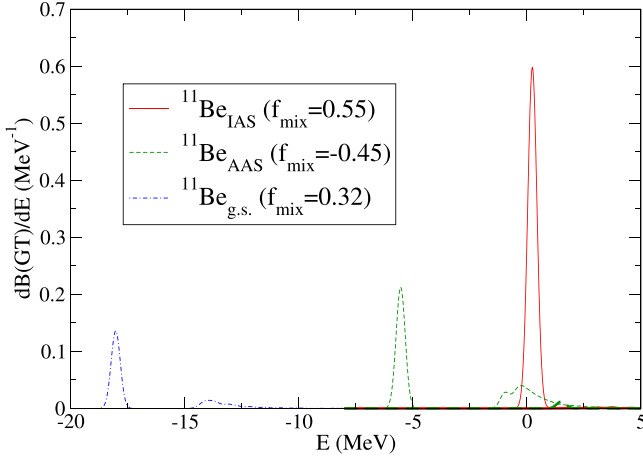
FIG. 5. Gamow-Teller strength, Eq. (24), for decay of $^{11}\text{Li}_{\text{g.s.}}$ into states, bound and continuum, with the same quantum numbers as $^{11}\text{Be}_{\text{IAS}}$ (solid curves), $^{11}\text{Be}_{\text{AAS}}$ (dashed curves), and $^{11}\text{Be}_{\text{g.s.}}$ (dot-dashed curves), as a function of the energy of the final state. The mixing factor, f_{mix}, is equal to 0.55, −0.45, and 0.32, for each of the three cases, respectively. The hardly visible thick curves in the low-right corner show the very small contribution from the decay of the halo neutrons.

has to recall that f_{fin} is equal to $\sqrt{3/5}$, $-\sqrt{2/5}$, and 1 for each of the transitions mentioned above (third column in Table IV).

Using the f_{mix} values given above, we obtain the computed Gamow-Teller strengths, Eq. (24), shown in Fig. 5 for decay of $^{11}\text{Li}_{\text{g.s.}}$ into states, bound and continuum, with the same quantum numbers as $^{11}\text{Be}_{\text{IAS}}$ (solid curves), $^{11}\text{Be}_{\text{AAS}}$ (dashed curves), and $^{11}\text{Be}_{\text{g.s.}}$ (dot-dashed curves). The thick curves in the low-right corner of the figure show the tiny contribution to the strength from the β decay of the halo neutrons (which is exactly zero for the case of decay into $^{11}\text{Be}_{\text{g.s.}}$). This contribution is hardly visible, and the consequence is that the curves in Fig. 5 are simply the ones in Fig. 4 scaled by the factor f_{mix}^2. As a consequence, the integrals under the curves is nothing but the product of f_{min}^2 and the values of B_{ov} given in Table III. In this way we get the total Gamow-Teller strengths 0.30, 0.18, and 0.09 for transitions into $^{11}\text{Be}_{\text{IAS}}$, $^{11}\text{Be}_{\text{AAS}}$, and $^{11}\text{Be}_{\text{g.s.}}$, respectively, from which 0.29, 0.10, and 0.07 correspond to transitions into the noncontinuum IAS, AAS, and $^{11}\text{Be}_{\text{g.s.}}$, and the rest is given by decay into the continuum. These results have been collected into the lower part of Table V, where the last row gives the f_{mix} values used, and where, for completeness, we also give the strengths for Fermi decay.

VII. COMPARISON TO DATA

A brief overview of the current experimental state of knowledge on the β decay of ^{11}Li and its core ^9Li is given in Appendix D and Fig. 7. Here we emphasize those aspects that are relevant to compare with our calculations.

A. Three-body energies

Our calculations should be most reliable for the $3/2^-$ IAS and AAS. The IAS energy has been adjusted to the

TABLE V. Integrated strengths for Fermi and Gamow-Teller decay of $^{11}\text{Li}_{\text{g.s.}}$ into $^{11}\text{Be}_{\text{IAS}}$, $^{11}\text{Be}_{\text{AAS}}$, and $^{11}\text{Be}_{\text{g.s.}}$. For the case of Gamow-Teller decay we split the total strength into the contributions from the noncontinuum states and the continuum background. The last row gives the f_{mix} values, Eq. (34), used to compute the Gamow-Teller strengths.

	$^{11}\text{Be}_{\text{IAS}}$	$^{11}\text{Be}_{\text{AAS}}$	$^{11}\text{Be}_{\text{g.s.}}$
Fermi	5.0	0	0
Gamow-Teller	0.30	0.18	0.09
GT (no cont.)	0.29	0.10	0.07
GT (continuum)	<0.01	0.08	0.02
f_{mix}	0.55	−0.45	0.32

experimental position at 21.16 MeV as determined in a charge-reaction experiment [25], but neither the total strength nor the isospin purity could be accurately extracted in the experiment. The AAS position is then predicted to be at 15.39 MeV (see Table II), which fits naturally with the experimentally established $3/2^-$ level at 16.3 MeV.

B. The IAS and AAS strengths

The Fermi strength of 5 to the IAS is significantly larger than the predicted Gamow-Teller strength of 0.29 and will dominate the transition. The transition is not energetically allowed in β decay and it has not been possible to extract an accurate strength from the existing charge-reaction experiment. The predicted GT β strength to the AAS is 0.10 and thereby close to the so far identified experimental strength of 0.12. We note that not all experimental strength may have been identified yet and that the Fermi strength is negligible. The predicted isospin impurity of the IAS, 3.7×10^{-3}, is large for such a light nucleus, but still too small to be easily measured. The magnitude is, as is the mismatch of 0.02 in the spatial overlap ^{11}Li to IAS of 0.98, increased due to the halo structure.
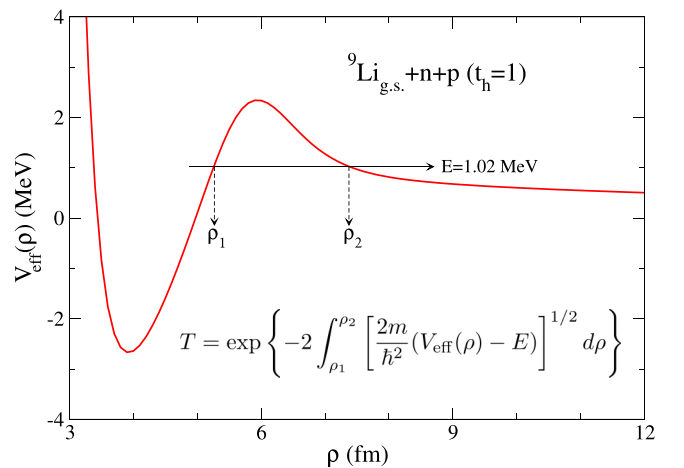

FIG. 6. Lowest effective potential for the $^9\text{Li}_{\text{g.s.}} + n + p$ system with $t_h = 1$, and turning points, ρ_1 and ρ_2, for the energy of the $^{11}\text{Be}_{\text{IAS}}$ state. The WKB transmission coefficient through the barrier, T, is obtained as indicated in the figure.
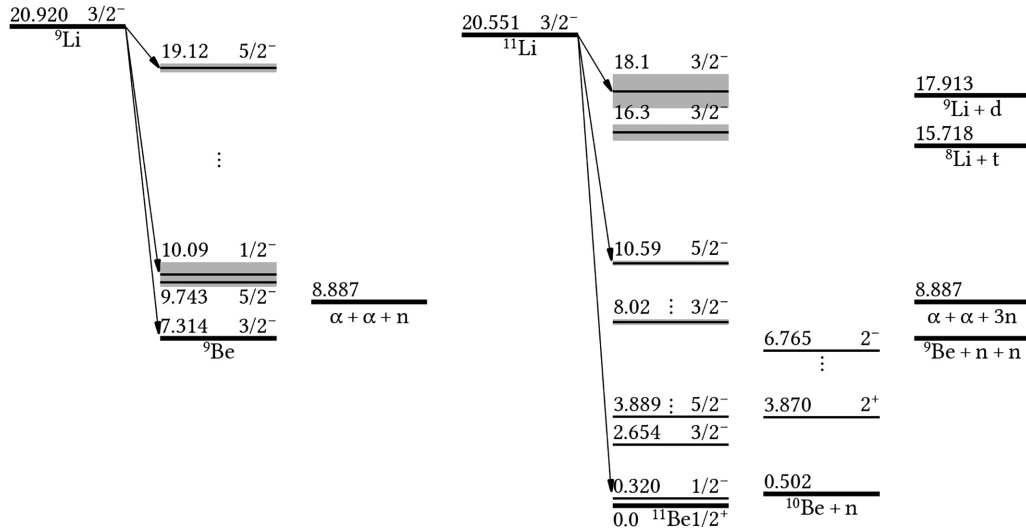
FIG. 7. Comparison of the β decays of ^{9}Li and ^{11}Li. A selection of states fed in the decays is shown along with important thresholds for particle emission.

C. Decay branches

As shown in Eq. (28), the IAS contains two different three-body components, the ^{9}Be$_{\text{IAS}}$ $+n+n$ and the ^{9}Li$_{\text{g.s.}}$ $+n+p$ structures, both with $t_h = 1$. As seen in Fig. 1, the IAS energy is below the ^{9}Be$_{\text{IAS}}$ $+n+n$ threshold by 0.55 MeV, but above the ^{9}Li$_{\text{g.s.}}$ $+n+p$ threshold by 1.02 MeV. Therefore, whereas the IAS can not decay through the ^{9}Be$_{\text{IAS}}$ $+n+$ n channel, it actually can do it through the ^{9}Li$_{\text{g.s.}}$ $+n+p$ channel. An estimate of the width for this decay can be obtained by means of the Wentzel-Kramers-Brillouin (WKB) approximation, as described in Ref. [26]. In Fig. 6 we show the lowest effective potential for the ^{9}Li$_{\text{g.s.}}$ $+n+p$ ($t_h = 1$) system, obtained with potential (i), given in Table I, and indicate the turning points, ρ_1 and ρ_2, corresponding to the IAS excitation energy. The transmission coefficient through the barrier, T, is obtained as indicated in the figure. The width, Γ, is then estimated as $\Gamma/\hbar = fT$, where the knocking rate, f, is obtained as $f = v/\rho_1$, and the velocity v is extracted after equating the kinetic energy, $mv^2/2$, and the energy difference between E and the maximum depth of the effective potential. Following this procedure we have obtained a WKB estimate for the width of the IAS of about 0.5 MeV, which agrees nicely with the experimental width, Ref. [25], of 0.49(7) MeV.

We do not predict strong particle decay branches from our AAS state, but as remarked earlier it is likely to mix with close-lying states of the same spin-parity. We therefore expect its decay pattern to be very similar to that of the 18 MeV level, an expectation that agrees with the current experimental knowledge [7].

Moving now to the ^{11}Be$_{\text{g.s.}}$ calculations, they are based on a shell-model strength for the ^{9}Be ground state transition that is a factor 4 above the experimental value. Our above predictions of a Gamow-Teller strength of 0.07 to a level at 2.89 MeV excitation energy in ^{11}Be and a strength of 0.02 situated around the $2n$ threshold (see Table V) should therefore be scaled down and are then below the experimental strength of 0.075 to

the $3/2^-$ levels at 2.69 and 3.97 MeV. We shall return below to the question of what the origin of the strength to the low-lying states in ^{11}Be is. Still, we note that Fig. 5 predicts strength to the states just below the one-neutron threshold in ^{10}Be as well as strength going directly to the two-neutron continuum. The barely bound states are experimentally known to be fed and have been proposed to have halo structure causing them to be preferentially fed in the ^{11}Li decay; see [27] and references therein. Here again the experimental strength points to the presence of other contributions.

D. Core decay

Model calculations for core decays into excited ^{9}Be states would require five-body calculations and are not currently doable. The following observations are therefore of a more speculative nature: Both decaying nuclei, ^{9}Li and ^{11}Li have large Q values with low particle separation energies in the daughter nuclei and final states that in many cases can be considered composed of α particles and neutrons. The observable β strength will be concentrated at high excitation energy and therefore clearly in the continuum. The spatial extension of the halo neutrons will tend to have larger overlap with final nucleons at low energy whereas the excitation energy residing in the core will be higher. The (final state) interactions between nucleons and α particles are strong at relative energies up to a few MeV, so it is not surprising that final states in the ^{9}Li decay tend to cluster into intermediate ^{8}Be $+n$ and ^{5}He $+\alpha$ states; see, e.g., Fig. 1 in [28]. A similar clustering has been found [29] for ^{11}Li decays into two charged fragments where final state ^{4}He $+$ ^{7}He structures have been clearly seen and there is evidence also for a ^{6}He(2^+) $+$ ^{5}He channel; both configurations appear by adding two neutrons to one fragment in the α + ^{5}He channel. The different final channels may be difficult to distinguish at low total energies, so the first few MeV above the two-neutron threshold in ^{11}Be could be challenging experimentally as well as numerically.

The first excited state in ^{9}Be fed in β decay is the narrow [0.78(13) keV] $5/2^-$ level at 2.43 MeV where the $B(GT)$ is 0.046(5) [20]. This could correspond to the $5/2^-$ 10.6 MeV level in ^{11}Be (see Fig. 7) to which the branching ratio seems to be around 2% (adding the values in [27,29], the branching ratio from [30] is higher, but is inconsistent with the data of [29]) giving a $B(GT)$ around 0.1.

The second state fed in ^{9}Be is the very broad [1.08(11) MeV] $1/2^-$ level at 2.78 MeV. It is the only $1/2^-$ level fed in the ^{9}Li decay and has a strong $2\alpha + n$ clustering. A ^{11}Li β decay with this "core component" would naturally lead to $2\alpha + 3n$ final configurations. The higher-lying states fed in ^{9}Be are also broad and would also be expected to lead to high-lying multibody final states. As a rough indicator, the partial half-life for all excited states in ^{9}Be, all leading to $2\alpha + n$, is around 350 ms, which would correspond to a ^{11}Li branching ratio of 2.5% that is close to $P_{3n} = 1.9(2)\%$. This lends support to the suggested parallel between the ^{9}Li and ^{11}Li decays.

The main fact opposing this suggested parallel is that the spin-parity of the strongly fed 11.8 MeV state in ^{9}Be is $5/2^-$, whereas the corresponding strongly fed 18 MeV state in ^{11}Be is reported as $3/2^-$; see Fig. 7. Both spin determinations come from angular distributions, assuming the decay channels could be clearly separated. If this discrepancy is confirmed when a better decay scheme is established, a core-decay scenario would be excluded.

E. Decay into $t_h = 0$ components

Finally, let us consider the additional halo decay components. The IAS and AAS correspond to $t_h = 1$ final state components. Decay into the $t_h = 0$ components ($T = \frac{3}{2}$, $T_z = -\frac{3}{2}$) will include core-deuteron structures. These states can be populated after Gamow-Teller β decay of ^{11}Li$_{g.s.}$, and the corresponding strength will be given by the first term in Eq. (22) only, i.e., the daughter nucleus is populated by decay of one of the halo neutrons in ^{11}Li$_{g.s.}$.

In Fig. 8 we plot the Gamow-Teller strength for decay of ^{11}Li$_{g.s.}$ into $t_h = 0$ states in ^{11}Be with total angular momentum and parity $J^\pi = 3/2^-$ (solid), $J^\pi = 1/2^-$ (dashed), and $J^\pi = 5/2^-$ (dotted). In the case of $J^\pi = 5/2^-$ there is a ^{11}Be state about 0.8 MeV below the ^{9}Li$_{g.s.}$ +deuteron threshold, which is responsible for the large peak observed in the dotted curve. For the other two cases, $J^\pi = 1/2^-$ and $J^\pi = 3/2^-$, all the computed states are found above the deuteron threshold. The sum of the three terms is shown by the thin-solid curve. The total integrated Gamow-Teller strengths are 1.21, 0.65, and 1.88 for the $3/2^-$, $1/2^-$, and $5/2^-$ cases, respectively. There is at the moment no experimental evidence for the $5/2^-$ level below the threshold, but decays directly to the deuteron continuum have been seen, the latest experiment [5,31] observing deuterons in the energy range 0.2 to 1.6 MeV above the deuteron threshold with a total experimental $B(GT)$ of 0.7 [5]. These experimental data are shown by the dots in the figure. The predicted integrated strengths in this range are 0.52, 0.25, and 0.11 for the $3/2^-$, $1/2^-$, and $5/2^-$ cases, respectively. The sum of 0.88 is slightly above the
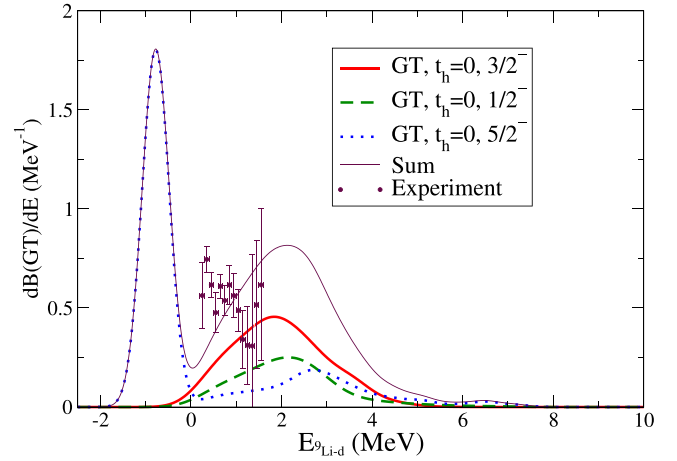

FIG. 8. Gamow-Teller strength, Eq. (24), for decay of ^{11}Li$_{g.s.}$ into $t_h = 0$ states in ^{11}Be with total angular momentum and parity $J^\pi = \frac{3}{2}^-$ (solid), $J^\pi = \frac{1}{2}^-$ (dashed), and $J^\pi = \frac{5}{2}^-$ (dotted). The sum of the three terms is shown by the brown (thin solid) curve. The strength is given as a function of the relative ^{9}Li$_{g.s.}$-deuteron energy. The experimental data are from [5,31].

experimental value and the theoretical strength increases with energy whereas the experimental is close to constant.

F. Decays outside the model

What remains is the decays that are outside our model space, namely the final states containing proton $p_{3/2}$ states fed by decay of a $p_{1/2}$ neutron. The $\boldsymbol{\sigma}$ operator favors the $p_{1/2}$ to $p_{3/2}$ transition over $p_{1/2}$ to $p_{1/2}$. For a simple estimate, the existing proton in ^{11}Li will block one out of the four $p_{3/2}$ substates and the two protons will couple to 0^+ or 2^+; these states in ^{10}Be can then couple with the remaining $p_{1/2}$ neutron to give $1/2^-$ or $3/2^-$ and $5/2^-$ states, respectively. The former could explain the feeding to the first excited ^{11}Be state [19], the latter will contribute to the excited states up to around 9 MeV.

We have calculated the one-particle wave function overlap between a ^{11}Li $p_{1/2}$ neutron and a well-bound proton or the halo neutron in the first excited ^{11}Be state to be 0.75 and 0.96, respectively. The $(p_{1/2})^2$ fraction in ^{11}Li is 0.35, the $p_{1/2}$ to $p_{3/2}$ fraction is 8/9; adding the Pauli blocking, the Gamow-Teller quenching and the wave function overlap all in all reduces the total halo strength of 6 to around 0.9. The sum of the currently assigned experimental strength to this region is around 0.6, which is in fair agreement.

VIII. CONCLUSION

We have extended the theoretical description of three-body systems to include isospin explicitly, thereby allowing a treatment of β decay processes. The framework reproduces selected parts of the decay well, in particular the decay to the isobaric analog state. It is also expected to reproduce the main features of the decay to the antianalog state that, however, can mix with surrounding levels. A distinct advantage is the ability to treat decays (both weak and strong) to final continuum

states, thereby giving a full description of the decay process. This is important for decays of halo nuclei. We have applied the framework to the decay of ^{11}Li that is a challenging case due to the nonzero spin of the core, ^{9}Li, and to the many relevant final-state channels.

Our description of both the IAS and AAS, where we identify the latter as the 16.3 MeV resonance, in ^{11}Be is consistent with all existing experimental data. We adjust the position of the IAS and then predict the position of the AAS to be close to the experimental one. The decay width of the IAS matches the experiment, and the decay pattern of the AAS is close to that of the nearby 18 MeV level, as could be expected. We note that the different potentials for core nucleon systems with $t_{cN} = 2$ and $t_{cN} = 1$ have been fitted independently, but that the strengths of the central potentials for different angular momenta are consistent with the difference being due to a common isospin-isospin nucleon-nucleon potential, as discussed in Appendix A. Our predicted isospin mixing for the IAS of 3.7×10^{-3} is very large for a light nucleus and significantly larger than expected for more bound nuclei.

The core internal degrees of freedom are only taken crudely into account through the matrix elements for decay of ^{9}Li into ^{9}Be states, and we furthermore only calculate explicitly results for decays into the ^{9}Be ground state. Nevertheless, a consistent overall interpretation of the β decay of ^{11}Li emerges as follows: the core β decay explains much of the structure from around the two-neutron threshold up to the Q value. The decay to the ground state of ^{9}Be has low intensity [actually, the sum of B(GT) values to the lowest 9 MeV in ^{9}Be is of order 0.1, only] and will give a small contribution to the ^{11}Li decays to the lowest 9 MeV in ^{11}Be that has a summed B(GT) of order 0.6. These decays get a larger contribution from the decay of the $p_{1/2}^2$ halo component where a produced $p_{3/2}$ proton couples with the core to make intermediate ^{10}Be 0^+ and 2^+ states. Apart from the transition to the AAS mentioned above and the transition to the 18 MeV state that is assumed to correspond to the ^{9}Li transition to the 11.8 MeV state (note, however, the need for a reinvestigation of this particular branch), the other high β strength transition at high excitation is the β-delayed deuteron branch that is fairly well reproduced as a halo β decay.

The large Q_β value for ^{11}Li is explained by the fact that adding two neutrons to ^{9}Li produces a barely bound nucleus, whereas adding two neutrons to ^{9}Be gives a significant energy gain; see Fig. 7. The gain comes mainly from the first neutron that fills the $p_{3/2}$ neutron orbit, whereas the second neutron again produces barely bound states. The above interpretation of where core and halo decays proceed to nicely fit this observation.

There are several clear consequences of this interpretation that can be tested experimentally. In general, the spectator halo neutrons from core decays should give low-energy final state neutrons; this is consistent with the results from the two-neutron coincidence spectrum in [32] where the majority of the coincident neutrons lie below 2 MeV. A specific requirement is that the 11.8 MeV state in ^{9}Li must have spin $3/2^-$ rather than the current experimental value of $5/2^-$.

There is a need for improved experimental data on both Li decays. The current discrepancies for the decay scheme

of ^{11}Li must be resolved and more detailed data on decays feeding the two- and three-neutron unbound continuum would be very valuable, although challenging to obtain as neutron detection is difficult. For ^{9}Li it is important to look closer at the strength residing above 10 MeV, both in order to resolve the puzzle of the spin of the 11.8 MeV level and in order to determine whether other levels contribute as predicted by several models. A renewed look at and comparison with the mirror decay of ^{9}C may be useful.

The β decay of ^{11}Li is challenging for several reasons. It would be interesting to test the methods developed here to decays of other drip line nuclei that can be described with few-body methods.

APPENDIX A: ISOSPIN AND INTERACTIONS

The basic nucleon-nucleon interaction contains isospin-isospin terms, e.g., from one-pion exchange, and as Lane [33] pointed out this will, for a system with one nucleon outside a core. give an interaction term $(U/A_c) \, \boldsymbol{t} \cdot \boldsymbol{t}_c$ where the constant U in mid-mass nuclei is of order 100 MeV. Robson [34] showed how this naturally leads to isobaric analog states of high purity, and also noted that the isospin mixing mainly arises from the region external to the nucleus. These argument can be generalized to our case. The isospin-isospin interaction for a two-neutron halo will have the form $(U/A)(\boldsymbol{t}_2 \cdot \boldsymbol{t}_c + \boldsymbol{t}_3 \cdot \boldsymbol{t}_c + \boldsymbol{t}_2 \cdot \boldsymbol{t}_3) = (U/A)(\boldsymbol{t}_h \cdot \boldsymbol{t}_c + \boldsymbol{t}_2 \cdot \boldsymbol{t}_3)$. Here the first term can be rewritten as $\boldsymbol{t}_h \cdot \boldsymbol{t}_c = 1/2(t_h^+ t_c^- + t_h^- t_c^+) + t_h^z t_c^z$. It is straightforward to verify that the explicit charge-exchange terms will transform the two components of the wave functions in Eqs. (3) and (4) into each other and thereby, in the absence of isospin-breaking terms in the Hamiltonian, enforce the structure of the IAS and the AAS.

The AAS is established in many light nuclei, e.g. in ^{12}C, where it is situated at 12.71 MeV, somewhat below the IAS at 15.11 MeV. It is known to play a role in both γ and β decays (see, e.g., the contributions in [35]), and often gives the main contribution to isospin purity violation [36].

The spatial and spin parts of the wave functions should have the same structure for the IAS and the AAS [the spatial extent can differ, as shown in Fig. 2(b)], and a substantial part of the difference in their energies will therefore come from the isospin-isospin interaction. For a two-neutron halo the $\boldsymbol{t}_2 \cdot \boldsymbol{t}_3$ term gives the same contribution in the two states, so the relevant quantity is the expectation value of $\boldsymbol{t}_h \cdot \boldsymbol{t}_c$. This differs by $t_h + t_c$ between the AAS and the IAS. However, the effective value of U will be less than that for bulk nuclear matter: we are in light nuclei and furthermore are dealing with loosely bound structures, so since the nucleon-nucleon isospin-isospin interaction is of short range its average value will fall below a simple $1/A$ scaling. The value of $E_{\text{IAS}} - E_{\text{AAS}} = (U_{\text{eff}}/A_c)(t_h + t_c)$ may be estimated from ^{12}C. Scaling

with mass number and isospin this would give a difference of about 7 MeV between the IAS and the AAS of ^{11}Li, a value that should be taken as an upper limit since the effect of the halo extension is not considered.

In our two-body potentials in Sec. V A we have not employed any isospin dependent potential, but rather deduced potentials for each isospin sector. It is therefore interesting that the difference in the strengths for $t_{cN} = 2$ and $t_{cN} = 1$ in Table I is of similar order of magnitude for the central potential, consistent with the isospin dependence being effectively included.

APPENDIX B: POTENTIAL MATRIX ELEMENTS FOR ^{11}Li$_{\text{g.s.}}$, ^{11}Be$_{\text{g.s.}}$, ^{11}Be$_{\text{IAS}}$, and ^{11}Be$_{\text{AAS}}$

Here we specify how the matrix elements of the core-nucleon potentials in between the different terms of the basis set $\{|\mathcal{Y}_q\rangle |T T_z\rangle\}$ are computed for the particular cases of ^{11}Li$_{\text{g.s.}}$, ^{11}Be$_{\text{g.s.}}$, ^{11}Be$_{\text{IAS}}$, and ^{11}Be$_{\text{AAS}}$.

From Eq. (12) we immediately get that, after rotation from the first to the second Jacobi set, the isospin wave functions for the ^{11}Li$_{\text{g.s.}}$, ^{11}Be$_{\text{g.s.}}$, ^{11}Be$_{\text{IAS}}$, and ^{11}Be$_{\text{AAS}}$ states are given by

$$|^{11}\text{Li}_{\text{g.s.}}\rangle = \left|(t_2, t_3)t_h = 1, t_c = \tfrac{3}{2}; T = \tfrac{5}{2}, T_z = -\tfrac{5}{2}\right\rangle = \left|(t_3, t_c)t_{cN} = 2, t_2 = \tfrac{1}{2}; T = \tfrac{5}{2}, T_z = -\tfrac{5}{2}\right\rangle, \tag{B1}$$

$$|^{11}\text{Be}_{\text{g.s.}}\rangle = \left|(t_2, t_3)t_h = 1, t_c = \tfrac{1}{2}; T = \tfrac{3}{2}, T_z = -\tfrac{3}{2}\right\rangle = \left|(t_3, t_c)t_{cN} = 1, t_2 = \tfrac{1}{2}; T = \tfrac{3}{2}, T_z = -\tfrac{3}{2}\right\rangle, \tag{B2}$$

$$|^{11}\text{Be}_{\text{IAS}}\rangle = \left|(t_2, t_3)t_h = 1, t_c = \tfrac{3}{2}; T = \tfrac{5}{2}, T_z = -\tfrac{3}{2}\right\rangle = \left|(t_3, t_c)t_{cN} = 2, t_2 = \tfrac{1}{2}; T = \tfrac{5}{2}, T_z = -\tfrac{3}{2}\right\rangle, \tag{B3}$$

$$|^{11}\text{Be}_{\text{AAS}}\rangle = \left|(t_2, t_3)t_h = 1, t_c = \tfrac{3}{2}; T = \tfrac{3}{2}, T_z = -\tfrac{3}{2}\right\rangle$$
$$= \sqrt{\tfrac{5}{8}}\left|(t_3, t_c)t_{cN} = 1, t_2 = \tfrac{1}{2}; T = \tfrac{3}{2}, T_z = -\tfrac{3}{2}\right\rangle - \sqrt{\tfrac{3}{8}}\left|(t_3, t_c)t_{cN} = 2, t_2 = \tfrac{1}{2}; T = \tfrac{3}{2}, T_z = -\tfrac{3}{2}\right\rangle, \tag{B4}$$

where we can see that ^{11}Li$_{\text{g.s.}}$ and ^{11}Be$_{\text{IAS}}$ can only hold $t_{cN} = 2$ values (otherwise the total isospin $T = \tfrac{5}{2}$ could not be reached) and the ^{11}Be$_{\text{g.s.}}$ can only have $t_{cN} = 1$ (otherwise the total isospin $T = \tfrac{3}{2}$ could not be reached). In contrast, ^{11}Be$_{\text{AAS}}$ mixes two different t_{cN} values, $t_{cN} = 1$ and $t_{cN} = 2$.

From the expressions above, and making use of Eq. (13), we can split the matrix elements corresponding to the core-nucleon interaction into the different t_{cN} parts:

$$\langle \mathcal{Y}_q \, ^{11}\text{Li}_{\text{g.s.}} |V_{cN}|\mathcal{Y}_{q'} \, ^{11}\text{Li}_{\text{g.s.}}\rangle = \langle \mathcal{Y}_q; (t_3, t_c)t_{cN} = 2, t_2 = \tfrac{1}{2}; \tfrac{5}{2}, -\tfrac{5}{2}|V_{cN}^{(t_{cN}=2)}|\mathcal{Y}_{q'}; (t_3, t_c)t_{cN} = 2, t_2 = \tfrac{1}{2}; \tfrac{5}{2}, -\tfrac{5}{2}\rangle, \tag{B5}$$

$$\langle \mathcal{Y}_q \, ^{11}\text{Be}_{\text{g.s.}} |V_{cN}|\mathcal{Y}_{q'} \, ^{11}\text{Be}_{\text{g.s.}}\rangle = \langle \mathcal{Y}_q; (t_3, t_c)t_{cN} = 1, t_2 = \tfrac{1}{2}; \tfrac{3}{2}, -\tfrac{3}{2}|V_{cN}^{(t_{cN}=1)}|\mathcal{Y}_{q'}; (t_3, t_c)t_{cN} = 1, t_2 = \tfrac{1}{2}; \tfrac{3}{2}, -\tfrac{3}{2}\rangle, \tag{B6}$$

$$\langle \mathcal{Y}_q \, ^{11}\text{Be}_{\text{IAS}} |V_{cN}|\mathcal{Y}_{q'} \, ^{11}\text{Be}_{\text{IAS}}\rangle = \langle \mathcal{Y}_q; (t_3, t_c)t_{cN} = 2, t_2 = \tfrac{1}{2}; \tfrac{5}{2}, -\tfrac{3}{2}|V_{cN}^{(t_{cN}=2)}|\mathcal{Y}_{q'}; (t_3, t_c)t_{cN} = 2, t_2 = \tfrac{1}{2}; \tfrac{5}{2}, -\tfrac{3}{2}\rangle, \tag{B7}$$

and

$$\langle \mathcal{Y}_q \, ^{11}\text{Be}_{\text{AAS}} |V_{cN}|\mathcal{Y}_{q'} \, ^{11}\text{Be}_{\text{AAS}}\rangle = \tfrac{5}{8}\langle \mathcal{Y}_q; (t_3, t_c)t_{cN} = 1, t_2 = \tfrac{1}{2}; \tfrac{3}{2}, -\tfrac{3}{2}|V_{cN}^{(t_{cN}=1)}|\mathcal{Y}_{q'}; (t_3, t_c)t_{cN} = 1, t_2 = \tfrac{1}{2}; \tfrac{3}{2}, -\tfrac{3}{2}\rangle$$
$$+ \tfrac{3}{8}\langle \mathcal{Y}_q; (t_3, t_c)t_{cN} = 2, t_2 = \tfrac{1}{2}; \tfrac{3}{2}, -\tfrac{3}{2}|V_{cN}^{(t_{cN}=2)}|\mathcal{Y}_{q'}; (t_3, t_c)t_{cN} = 2, t_2 = \tfrac{1}{2}; \tfrac{3}{2}, -\tfrac{3}{2}\rangle \tag{B8}$$

where we have assumed that the potential does not mix different values of the core-nucleon isospin, t_{cN}.

Finally, from Eq.(14) we can find the specific core-nucleon states, and therefore the specific core-nucleon interactions, involved in the different three-body systems under consideration:

$$\langle \mathcal{Y}_q; ^{11}\text{Li}_{\text{g.s.}} |V_{cN}|\mathcal{Y}_{q'}; ^{11}\text{Li}_{\text{g.s.}}\rangle = \langle \mathcal{Y}_q; ^{9}\text{Li}_{\text{g.s.}} + n|V_{cN}^{(t_{cN}=2)}|\mathcal{Y}_{q'}; ^{9}\text{Li}_{\text{g.s.}} + n\rangle, \tag{B9}$$

$$\langle \mathcal{Y}_q; ^{11}\text{Be}_{\text{g.s.}} |V_{cN}|\mathcal{Y}_{q'}; ^{11}\text{Be}_{\text{g.s.}}\rangle = \langle \mathcal{Y}_q; ^{9}\text{Be}_{\text{g.s.}} + n|V_{cN}^{(t_{cN}=1)}|\mathcal{Y}_{q'}; ^{9}\text{Be}_{\text{g.s.}} + n\rangle, \tag{B10}$$

$$\langle \mathcal{Y}_q \, ^{11}\text{Be}_{\text{IAS}} |V_{cN}|\mathcal{Y}_{q'} \, ^{11}\text{Be}_{\text{IAS}}\rangle = \tfrac{1}{5}\langle \mathcal{Y}_q; ^{9}\text{Li}_{\text{g.s.}} + n|V_{cN}^{(t_{cN}=2)}|\mathcal{Y}_{q'}; ^{9}\text{Li}_{\text{g.s.}} + n\rangle + \tfrac{1}{5}\langle \mathcal{Y}_q; ^{9}\text{Li}_{\text{g.s.}} + p|V_{cN}^{(t_{cN}=2)}|\mathcal{Y}_{q'}; ^{9}\text{Li}_{\text{g.s.}} + p\rangle$$
$$+ \tfrac{3}{5}\langle \mathcal{Y}_q; ^{9}\text{Be}_{\text{IAS}} + n|V_{cN}^{(t_{cN}=2)}|\mathcal{Y}_{q'}; ^{9}\text{Be}_{\text{IAS}} + n\rangle, \tag{B11}$$

$$\langle \mathcal{Y}_q \, ^{11}\text{Be}_{\text{AAS}} |V_{cN}|\mathcal{Y}_{q'} \, ^{11}\text{Be}_{\text{AAS}}\rangle = \tfrac{5}{32}\langle \mathcal{Y}_q; ^{9}\text{Be}_{\text{IAS}} + n|V_{cN}^{(t_{cN}=1)}|\mathcal{Y}_{q'}; ^{9}\text{Be}_{\text{IAS}} + n\rangle + \tfrac{9}{160}\langle \mathcal{Y}_q; ^{9}\text{Be}_{\text{IAS}} + n|V_{cN}^{(t_{cN}=2)}|\mathcal{Y}_{q'}; ^{9}\text{Be}_{\text{IAS}} + n\rangle$$
$$+ \tfrac{15}{32}\langle \mathcal{Y}_q; ^{9}\text{Li}_{\text{g.s.}} + p|V_{cN}^{(t_{cN}=1)}|\mathcal{Y}_{q'}; ^{9}\text{Li}_{\text{g.s.}} + p\rangle + \tfrac{3}{160}\langle \mathcal{Y}_q; ^{9}\text{Li}_{\text{g.s.}} + p|V_{cN}^{(t_{cN}=2)}|\mathcal{Y}_{q'}; ^{9}\text{Li}_{\text{g.s.}} + p\rangle$$
$$+ \tfrac{3}{10}\langle \mathcal{Y}_q; ^{9}\text{Li}_{\text{g.s.}} + n|V_{cN}^{(t_{cN}=2)}|\mathcal{Y}_{q'}; ^{9}\text{Li}_{\text{g.s.}} + n\rangle. \tag{B12}$$

Therefore, the required interactions are (*i*) The interaction between the ^{9}Li$_{\text{g.s.}}$ core and the neutron (only $t_{cN} = 2$ is possible), (*ii*) the interaction between the ^{9}Be$_{\text{g.s.}}$ core and the neutron (only $t_{cN} = 1$ is possible), (*iii*) the interaction between the ^{9}Li$_{\text{g.s.}}$ core and the proton for $t_{cN} = 2$, (*iv*) the interaction between the ^{9}Be$_{\text{IAS}}$ core and the neutron for $t_{cN} = 2$, (*v*) the

interaction between the $^9\text{Li}_{\text{g.s.}}$ core and the proton for $t_{cN} = 1$, and (*vi*) the interaction between the $^9\text{Be}_{\text{IAS}}$ core and the neutron for $t_{cN} = 1$.

APPENDIX C: $\mathcal{H}_{\text{core}}$ MATRIX ELEMENTS FOR $^{11}\text{Li}_{\text{g.s.}}$, $^{11}\text{Be}_{\text{g.s.}}$, $^{11}\text{Be}_{\text{IAS}}$, and $^{11}\text{Be}_{\text{AAS}}$

Following Eq. (8), we have that the effect of the core hamiltonian, $\mathcal{H}_{\text{core}}$, on the different core states involved in the three-body systems considered in this work, can be expressed as

$$\mathcal{H}_{\text{core}}\left|t_c = \tfrac{3}{2}, t_c^z = -\tfrac{3}{2}\right\rangle = \mathcal{H}_{\text{core}}|^9\text{Li}_{\text{g.s.}}\rangle = \xi_{^9\text{Li}_{\text{g.s.}}}|^9\text{Li}_{\text{g.s.}}\rangle, \tag{C1}$$

$$\mathcal{H}_{\text{core}}\left|t_c = \tfrac{1}{2}, t_c^z = -\tfrac{1}{2}\right\rangle = \mathcal{H}_{\text{core}}|^9\text{Be}_{\text{g.s.}}\rangle = \xi_{^9\text{Be}_{\text{g.s.}}}|^9\text{Be}_{\text{g.s.}}\rangle, \tag{C2}$$

$$\mathcal{H}_{\text{core}}\left|t_c = \tfrac{3}{2}, t_c^z = -\tfrac{1}{2}\right\rangle = |^9\text{Be}_{\text{IAS}}\rangle = \xi_{^9\text{Be}_{\text{IAS}}}|^9\text{Be}_{\text{IAS}}\rangle, \tag{C3}$$

where $\xi_{^9\text{Li}_{\text{g.s.}}}$, $\xi_{^9\text{Be}_{\text{g.s.}}}$, and $\xi_{^9\text{Be}_{\text{IAS}}}$ are the energies of the $^9\text{Li}_{\text{g.s.}}$, $^9\text{Be}_{\text{g.s.}}$, and $^9\text{Be}_{\text{IAS}}$ cores, respectively.

Making now use of Eqs. (26) to (29), we can then easily get the matrix elements of $\mathcal{H}_{\text{core}}$ between the different terms of the basis set:

$$\langle \mathcal{Y}_q\,^{11}\text{Li}_{\text{g.s.}}\,|\mathcal{H}_{\text{core}}|\mathcal{Y}_{q'}\,^{11}\text{Li}_{\text{g.s.}}\rangle = \xi_{^9\text{Li}_{\text{g.s.}}}\delta_{qq'}, \tag{C4}$$

$$\langle \mathcal{Y}_q\,^{11}\text{Be}_{\text{g.s.}}\,|\mathcal{H}_{\text{core}}|\mathcal{Y}_{q'}\,^{11}\text{Be}_{\text{g.s.}}\rangle = \xi_{^9\text{Be}_{\text{g.s.}}}\delta_{qq'}, \tag{C5}$$

$$\langle \mathcal{Y}_q\,^{11}\text{Be}_{\text{IAS}}\,|\mathcal{H}_{\text{core}}|\mathcal{Y}_{q'}\,^{11}\text{Be}_{\text{IAS}}\rangle = \left(\tfrac{2}{5}\xi_{^9\text{Li}_{\text{g.s.}}} + \tfrac{3}{5}\xi_{^9\text{Be}_{\text{IAS}}}\right)\delta_{qq'}, \tag{C6}$$

$$\langle \mathcal{Y}_q\,^{11}\text{Be}_{\text{AAS}}\,|\mathcal{H}_{\text{core}}|\mathcal{Y}_{q'}\,^{11}\text{Be}_{\text{AAS}}\rangle = \left(\tfrac{3}{5}\xi_{^9\text{Li}_{\text{g.s.}}} + \tfrac{2}{5}\xi_{^9\text{Be}_{\text{IAS}}}\right)\delta_{qq'}, \tag{C7}$$

which are consistent with the general expressions given in Eqs.(9), (10), and (11). We have assumed that $\mathcal{H}_{\text{core}}$ does not mix the $^9\text{Li}_{\text{g.s.}}$ and $^9\text{Be}_{\text{IAS}}$ wave functions.

APPENDIX D: DECAY DATA FOR ^9Li AND ^{11}Li

Both decays involve broad (and partially overlapping) resonances in the daughter nuclei so that branching ratios and β strength may not always be uniquely attributed to a given level. A discussion is given in [37] that suggests considering $B(\text{GT})$ as a function of the final-state energy when comparing theory and experiment. For narrow levels the usual relation between $B(\text{GT})$ and the ft value is $ft = 6144(4)/[B(\text{F}) + (g_A/g_V)^2 B(\text{GT})]$, where the conversion factor is taken from superallowed Fermi transitions [38] and neutron decay gives $g_A/g_V = -1.2754(13)$ [39]. The empirical quenching factor for Gamow-Teller strength was for light nuclei estimated in [40] to be 0.845 and 0.833 for mass 9 and 11 nuclei, giving effective values for $(g_A/g_V)^2$ of 1.16 and 1.13 that we shall use when extracting experimental $B(\text{GT})$ values.

1. The ^9Li decay

A detailed overview of the current knowledge on the ^9Li decay can be found from [20,28]. It has historically been difficult to unravel the decays via excited ^9Be states, see Fig. 7, since the obvious decay channels, through $\alpha + {}^5\text{He}$ and through $n + {}^8\text{Be}$, lead to the same final continuum and can overlap in energy. The currently established branches go to the $3/2^-$ ground state and excited states at 2.43 MeV $(5/2^-)$, 2.8 MeV $(1/2^-)$, 5.0 MeV $(3/2^-)$, 7.9 MeV $(5/2^-)$, and 11.8 MeV $(5/2^-)$. The main Gamow-Teller strength goes to the 11.8 MeV state, but has been difficult to determine accurately; different approaches give numbers in the range 5 to 8. The ground state transition has a strength of 0.026(1) and the states in between have strengths of similar order of magnitude. For the five lowest states this is all very consistent with earlier theoretical treatments [6,8,40,41] that all predict several strong transitions in the energy range 10–13 MeV where only one has been observed.

2. The ^{11}Li decay

A good overview of the existing data on the ^{11}Li decay can be found in the review [42], the only more recent experimental result being the first hint at the energy distribution for two-neutron coincidences [32]. Most experiments have focused on the low-energy range, roughly up to around the two-neutron threshold in ^{11}Be, and the overall features of the decay are known here. However, the detailed interpretation differs between the most recent experiments [27,30] and there are still only few data from the higher-energy region, so the distribution of β strength is still uncertain. Figure 7 displays some of the levels that currently are believed to play a role in the decay.

Around 93% of the decay goes to neutron unbound states, the bound state feeding goes to the first excited $1/2^-$ halo state in ^{11}Be. The measurement of Hirayama *et al.* [30] detected neutrons as well as γ rays and β polarization. The extracted β asymmetry is for most neutron energies consistent with ^{11}Be spins of $3/2^-$ or $5/2^-$ (or a mixture of both); it is only in very small regions at high neutron energy that $1/2^-$ is indicated with perhaps an indication of a contribution also at low neutron energies. Their suggested level scheme differs in many details from the one extracted from the latest analysis [27] of β-n-γ decays, but agrees on including essentially the same $3/2^-$ and $5/2^-$ states up to 10.6 MeV. In terms of branching ratios they indicate that around 58% of the decays go to states below the two-neutron threshold, and around 32% to states above this up to the 10.6 MeV state. The total assigned probability for β-delayed one-neutron emission does not exceed 70%, which is considerably below the tabulated value of $P_{1n} = 86.3(9)\%$.

Only one β-n-γ experiment [43] reported neutrons from states at higher energies; the reported intensity of 6% does not include neutron emission to the ground state nor the branching of around 1% to n-α-^6He. The multineutron emission probabilities of $P_{2n} = 4.1(4)\%$ and $P_{3n} = 1.9(2)\%$ combined with the small fractions of order 10^{-4} going via βd and βt show that a sizable strength (and a non-negligible branching) will go to the multiparticle continuum. The most recent

measurements on branches with two charged particles [7,29] point to a significant role played by three levels, at 10.6 MeV, 16.3 MeV, and just above 18 MeV. The latter level has also been invoked in βt and βn branches, whereas the βd decay is normally assumed to proceed directly to the continuum. However, the overall experimental picture leaves many questions, in particular above the two-neutron threshold.

[1] A. S. Jensen, K. Riisager, D. V. Fedorov, and E. Garrido, Rev. Mod. Phys. **76**, 215 (2004).

[2] K. Riisager, Phys. Scr. **2013**, 014001 (2013).

[3] B. Blank and M. J. G. Borge, Prog. Part. Nucl. Phys. **60**, 403 (2008).

[4] M. Pfützner, M. Karny, L. V. Grigorenko, and K. Riisager, Rev. Mod. Phys. **84**, 567 (2012).

[5] K. Riisager, *Handbook of Nuclear Physics*, edited by I. Tanihata, H. Toki, and T. Kajino (Springer, Singapore, 2022).

[6] T. Suzuki and T. Otsuka, Phys. Rev. C **56**, 847 (1997).

[7] M. Madurga *et al.*, Phys. Lett. B **677**, 255 (2009).

[8] Y. Kanada-En'yo, Phys. Rev. C **81**, 034321 (2010).

[9] Y. Ohbayasi and Y. Suzuki, Phys. Lett. B **346**, 223 (1995).

[10] M. V. Zhukov, B. V. Danilin, L. V. Grigorenko, and J. S. Vaagen, Phys. Rev. C **52**, 2461 (1995).

[11] D. Baye, E. M. Tursunov, and P. Descouvemont, Phys. Rev. C **74**, 064302 (2006).

[12] E. Nielsen, D. V. Fedorov, A. S. Jensen, and E. Garrido, Phys. Rep. **347**, 373 (2001).

[13] E. Garrido and A. S. Jensen, Phys. Rev. C **101**, 034003 (2020).

[14] T. Nilsson, G. Nyman, and K. Riisager, Hyperfine Interact. **129**, 67 (2000).

[15] B. Jonson, Phys. Rep. **389**, 1 (2004).

[16] W. H. Press, S. A. Teukolsky, W. T. Vetterling, and B. P. Flannery, *Numerical Recipes in Fortran 77: The Art of Scientific Computing* (Cambridge University Press, Cambridge, 1997), Chap. 19.

[17] R. Álvarez-Rodríguez, A. S. Jensen, E. Garrido, and D. V. Fedorov, Phys. Rev. C **82**, 034001 (2010).

[18] H. Sagawa, I. Hamamoto, and M. Ishihara, Phys. Lett. B **303**, 215 (1993).

[19] T. Suzuki and T. Otsuka, Phys. Rev. C **50**, R555 (1994).

[20] D. R. Tilley, J. H. Kelley, J. L. Godwin, D. J. Millener, J. Purcell, C. G. Sheu, and H. R. Weller, Nucl. Phys. A **745**, 155 (2004).

[21] E. Garrido, D. V. Fedorov, and A. S. Jensen, Phys. Rev. C **69**, 024002 (2004).

[22] E. Garrido, D. V. Fedorov, and A. S. Jensen, Phys. Rev. C **68**, 014002 (2003).

[23] Y. Suzuki and K. Yabana, Phys. Lett. B **272**, 173 (1991).

[24] P. G. Hansen, A. S. Jensen, and K. Riisager, Nucl. Phys. A **560**, 85 (1993).

[25] T. Teranishi *et al.*, Phys. Lett. B **407**, 110 (1997).

[26] E. Garrido, D. V. Fedorov, and A. S. Jensen, Nucl. Phys. A **733**, 85 (2004).

[27] C. M. Mattoon, F. Sarazin, C. Andreoiu, A. N. Andreyev, R. A. E. Austin, G. C. Ball *et al.*, Phys. Rev. C **80**, 034318 (2009).

[28] Y. Prezado *et al.*, Phys. Lett. B **618**, 43 (2005).

[29] M. Madurga *et al.*, Nucl. Phys. A **810**, 1 (2008).

[30] Y. Hirayama *et al.*, Phys. Lett. B **611**, 239 (2005).

[31] R. Raabe, A. Andreyev, M. J. G. Borge, L. Buchmann, P. Capel, H. O. U. Fynbo *et al.*, Phys. Rev. Lett. **101**, 212501 (2008).

[32] F. Delaunay *et al.*, Nuovo Cimento **42C**, 98 (2019).

[33] A. M. Lane, Nucl. Phys. **35**, 676 (1962).

[34] D. Robson, Phys. Rev. **137**, B535 (1965).

[35] *Isospin in Nuclear Physics*, edited by D. H. Wilkinson (North-Holland, Amsterdam, 1969).

[36] V. Zelevinsky and A. Volya, *Physics of Atomic Nuclei* (Wiley-VCH, Weinheim, 2017), p. 40.

[37] K. Riisager, Nucl. Phys. A **925**, 112 (2014); **925**, 298 (2014).

[38] J. C. Hardy and I. S. Towner, Phys. Rev. C **102**, 045501 (2020).

[39] P. A. Zyla *et al.* (Particle Data Group), Prog. Theor. Exp. Phys. **2020**, 083C01 (2020).

[40] W. T. Chou, E. K. Warburton, and B. A. Brown, Phys. Rev. C **47**, 163 (1993).

[41] D. Mikolas *et al.*, Phys. Rev. C **37**, 766 (1988).

[42] J. H. Kelley *et al.*, Nucl. Phys. A **880**, 88 (2012).

[43] H. O. U. Fynbo *et al.*, Nucl. Phys. A **736**, 39 (2004).